Journal of Medicinal Chemistry

Article

Cite This: J. Med. Chem. 2018, 61, 2500−2517

pubs.acs.org/jmc

Targeting Multiple Effector Pathways in Pancreatic Ductal Adenocarcinoma with a G-Quadruplex-Binding Small Molecule

Chiara Marchetti,[†] Katherine G. Zyner,[‡] Stephan A. Ohnmacht,[†] Mathew Robson,[§] Shozeb M. Haider,[†] Jennifer P. Morton,[∥,⊥] Giovanni Marsico,[‡] Tam Vo,[#] Sarah Laughlin-Toth,[#] Ahmed A. Ahmed,[†] Gloria Di Vita,[†] Ingrida Pazitna,[†] Mekala Gunaratnam,[†] Rachael J. Besser,[†] Ana C. G. Andrade,[†] Seckou Diocou,[▽] Jeremy A. Pike,[‡,○] David Tannahill,[‡] R. Barbara Pedley,[▽] T. R. Jeffry Evans,[∥,⊥] W. David Wilson,[#] Shankar Balasubramanian,[‡,¶,◆] and Stephen Neidle*[,†]

[†]UCL School of Pharmacy, University College London, 29-39 Brunswick Square, London WC1N 1AX, U.K.

[‡]Cancer Research UK, Cambridge Research Institute, Li Ka Shing Centre, Robinson Way, Cambridge CB2 0RE, U.K.

[§]Cancer Research UK Cancer Centre, UCL Cancer Institute, University College London, London WC1E 6BT, U.K.

[∥]Cancer Research UK, Beatson Institute, Garscube Estate, Switchback Road, Glasgow G61 1BD U.K.

[⊥]Institute of Cancer Sciences. University of Glasgow, Glasgow G12 8QQ, U.K.

[#]Department of Chemistry and Center for Biotechnology and Drug Design, Georgia State University, Atlanta, Georgia 30303-3083, United States

[▽]UCL Cancer Institute, University College London, London WC1E 6BT, U.K.

[◆]Department of Chemistry, University of Cambridge, Cambridge CB2 1EW, U.K.

[¶]The School of Clinical Medicine, University of Cambridge, Cambridge CB2 0SP, U.K.

Supporting Information

ABSTRACT: Human pancreatic ductal adenocarcinoma (PDAC) involves the dysregulation of multiple signaling pathways. A novel approach to the treatment of PDAC is described, involving the targeting of cancer genes in PDAC pathways having over-representation of G-quadruplexes, using the trisubstituted naphthalene diimide quadruplex-binding compound 2,7-bis(3-morpholinopropyl)-4-((2-(pyrrolidin-1-yl)ethyl)amino)benzo[*lmn*][3,8]phenanthroline-1,3,6,8(2*H*,7*H*)-tetraone (CM03). This compound has been designed by computer modeling, is a potent inhibitor of cell growth in PDAC cell lines, and has anticancer activity in PDAC models, with a superior profile compared to gemcitabine, a commonly used therapy. Whole-transcriptome RNA-seq methodology has been used to analyze the effects of this quadruplex-binding small molecule on global gene expression. This has revealed the down-regulation of a large number of genes, rich in putative quadruplex elements and involved in essential pathways of PDAC survival, metastasis, and drug resistance. The changes produced by CM03 represent a global response to the complexity of human PDAC and may be applicable to other currently hard-to-treat cancers.

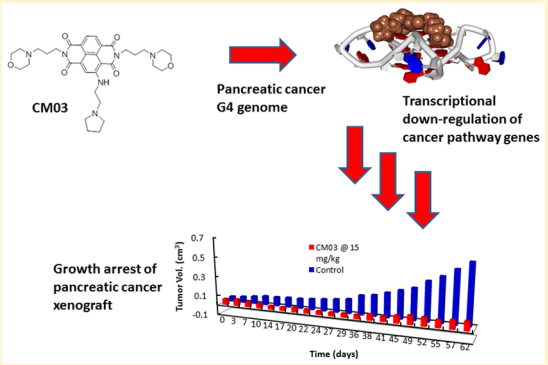

INTRODUCTION

Pancreatic cancer remains one of the most difficult to treat human cancers.[1] Pancreatic ductal adenocarcinomas (PDACs) comprise some 85% of diagnosed cases and are classified into several subtypes on the basis of expression analysis of major mutated genes.[2] PDACs typically have extensive patterns of germline mutations, especially in DNA repair and signaling pathways.[3,4] The most common mutations in PDACs are in the *KRAS*, *TP53*, *SMAD4*, and *CDKN2A* genes, with a lower frequency of mutations in many other genes.[3−6] A feature of PDACs is the distinctive pattern of changes in several gene pathways such as those involved in axon guidance and dysregulation of signal transduction via inhibition of Rho-GTPases.[6,7]

Only <4% of those diagnosed with stage III of PDAC survive for more than five years,[8,9] a situation that has not significantly changed for more than 40 years. Surgery is an option for <15−20% of cases, and chemotherapy for locally advanced inoperable or metastatic disease is still largely palliative. The nucleoside analogue gemcitabine remains a widely used monotherapy regimen used to treat PDAC.[10] Various formulations of gemcitabine and combinations with, in

Received: December 7, 2017
Published: January 22, 2018

DOI: 10.1021/acs.jmedchem.7b01781
J. Med. Chem. 2018, 61, 2500−2517

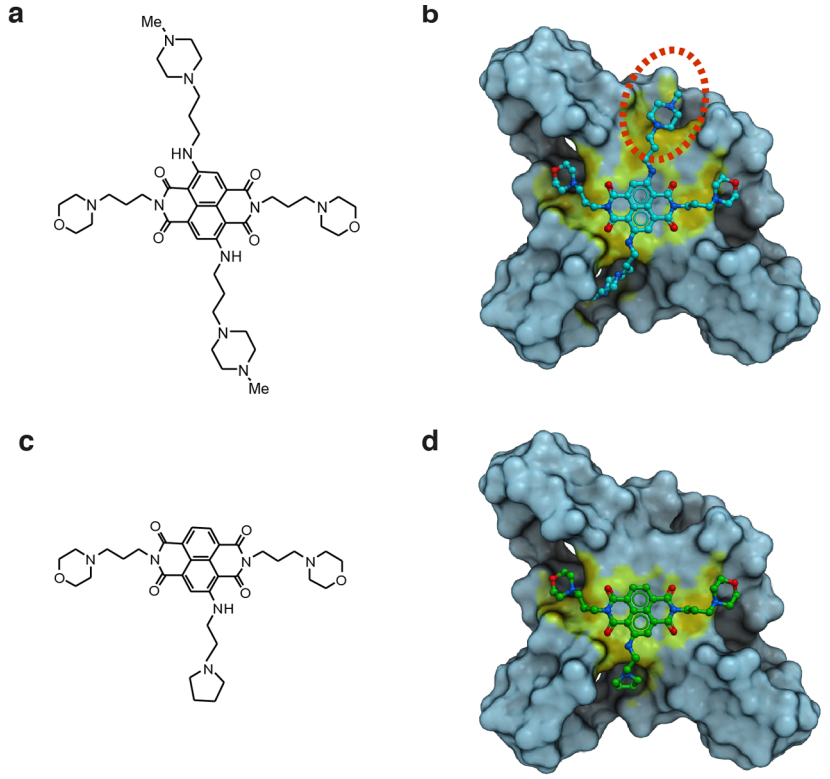

e

Changes in melting temperatures for G4 ligands determined by FRET

Drug	F21T	HSP90A	HSP90B	KRAS21	KRAS32	BCL-2	T-loop
CM03	11.8 ± 0.2	15.7 ± 0.2	12.7 ± 0.2	11.0 ± 0.2	9.6 ± 0.2	13.3 ± 0.2	0.6 ± 0.2
MM41	26.6 ± 0.2	33.1 ± 0.3	28.6 ± 0.2	22.5 ± 0.2	19.8 ± 0.2	26.4 ± 0.2	4.9 ± 0.2

f

Cell-line growth inhibition assay (IC_{50})

Drug	A549	MCF7	MIA PaCa-2	PANC-1	WI-38
CM03	24 ± 4	159 ± 20	7 ± 2	18 ± 3	1190 ± 21
MM41	19 ± 4	70 ± 10	11 ± 3	3 ± 1	230 ± 50

Figure 1. G4 modeling, FRET, and cell line growth inhibition studies of the trisubstituted naphthalene diimide derivatives MM41 and CM03. (a) MM41 structure and (b) molecular model of MM41 bound to a human telomeric G4, following docking and minimization and using the co-crystal structure (PDB 3UYH)[32a] as a starting point. The red dotted circle highlights the fourth pyrrolidino side chain substituent of MM41, which is not buried in a G4 groove, by contrast with the other three side chains. (c) CM03 structure and (d) molecular model of CM03 bound to the native parallel human telomeric G4 structure (PDB 1KF1)[32b] following docking and minimization. MM41 and CM03 are shown in ball-and-stick representation and the G4 in surface representation, with electrostatic interaction regions colored yellow. (e) Table showing melting temperature changes (ΔT_m) in °C, for CM03 and MM41 with a panel of G4s, determined using a FRET procedure performed in solution containing 50 mM K^+ ion. Ligands were used at 1 μM concentration. Standard deviations are from triplicate measurements. (f) Growth inhibition assays. Short-term 96 h IC_{50} values (in nM) for the two compounds in cancer and normal fibroblast cell line panel. Average growth inhibition is shown with standard deviations from >3 individual determinations.

particular, paclitaxel, have been developed; some have been in clinical trial,[11] and a small number have received regulatory approval[1] but their benefit is limited. The use of combination regimens of cytotoxic agents, as in the FOLFIRINOX (folinic acid + irinotecan + 5-fluorouracil + oxaliplatin) combination,[12] is restricted in use due to their toxicity. By contrast to other cancers, immunotherapy has not shown promising clinical results with PDAC,[1] possibly due to its inherent immunosuppression. Therapies based on the common mutations in pancreatic cancer that target hard-to-drug proteins such as KRAS have not yet reached the clinic, although recent results suggest promise for the future.[13]

Here, we report an alternative approach, of selectively targeting G-quadruplex (G4) elements in the genomes of pancreatic cancer cells. The human genome contains a large number of putative G4 sequences comprising several (typically four) short guanine tracts separated by more general sequence loops (reviewed in ref 14). G4 sequences are over-represented in promoters[15] and untranslated regions, particularly in genes associated with cell proliferation and cancer.[16,17] In principle, this over-representation in cancer-associated genes gives G4 targeting a therapeutic advantage, which can be emphasized by stabilizing individual G4 structures with an appropriate G4-selective small molecule. Visualization of G4s in cancer cells[18,19] and tissues[20] has further demonstrated their potential for selectivity. Many studies have examined the effects of such compounds on G4s within individual target genes,[21] arising from the concept that stabilization of a promoter G4 can result

DOI: 10.1021/acs.jmedchem.7b01781
J. Med. Chem. 2018, 61, 2500−2517

in inhibition of the expression of the gene involved.[22] A wide range of chemotypes as G4 stabilizers have been examined although they tend to share common structural features of an extended aromatic or heteroaromatic core with one or more cationic side chains.[21] Down-regulation of "targeted" genes such as *MYC*, *KIT*, *BCL2*, *VEGF*, and *KRAS* has often been reported (reviewed in ref 23), although unequivocal demonstrations of direct cause and effect at the cellular level have rarely been made.[24] The synthetic fluoroquinolone compound Quarfloxin (CX-3543)[25] has been evaluated in human cancer clinical trials, and its G4-binding was reported as inhibiting RNA biogenesis. More recently, another fluoroquinolone, CX-5461,[26] has been shown to be a G4-binding compound with selective effects in BRCA1/2-deficient cells; CX-5461 has recently entered clinical trials for patients with BRCA-deficient tumors.[27]

We have adopted a distinct approach in comparison to the single G4 promoter targeting strategy, in which we have not a priore assumed any particular promoter G4 targets. Instead, we have used global genome transcriptome profiling to determine which genes are affected by a rationally designed G4-binding small molecule. This has enabled us to determine potential targets at the whole genome level in two pancreatic cancer cell lines. We find that pancreatic cancer cell growth is especially sensitive to CM03 and that it strikingly inhibits tumor growth in PDAC animal models.

Naphthalene diimides are a favored chemotype for G4 binding because of their high target affinity, synthetic accessibility, and potential for chemical variability.[28,29] We have previously disclosed several focused libraries of naphthalene diimides, in particular, tetra-substituted analogues[30,31,32a,33] (Figure 1a) with molecular design based on crystallographic data for a series of G4–ligand complexes.[32a] We report here on a new lead compound, 2,7-bis(3-morpholinopropyl)-4-((2-(pyrrolidin-1-yl)ethyl)amino)benzo[*lmn*][3,8]phenanthroline-1,3,6,8(2*H*,7*H*)-tetraone (CM03, 633.34 Da; compound **4** in Scheme 1 and Figure 1c), which contains two side chains terminating in morpholino groups, a third side chain terminating in a protonated pyrrolidino group, and a lower molecular weight compared to the parent tetra-substituted compound MM41[32a] (831.08 Da; Figure 1a). We report here that CM03 (i) has potent growth inhibitory activity in vitro for pancreatic cancer cells, (ii) has antitumor activity in vivo in PDAC animal models, (iii) down-regulates the expression of key genes involved in maintaining the progression of PDAC and in drug resistance, and (iv) targets genes which have high G4 propensity.

Altogether these results demonstrate that G4 targeting is a realistic and attainable concept for potent G4-binding compounds, and has promise to lead to significant therapeutic advantage in the treatment of PDAC.

RESULTS

Design and Synthesis of the Trisubstituted Naphthalene Diimide Compound. The starting-point for CM03 design was the co-crystal structure of MM41 (Figure 1a,b), with an intramolecular human telomeric parallel G4. We reasoned that although the nature and structures of most potential target G4s are unknown, several features are common to all G4s, in particular a core of stacked G-quartets with small-molecule binding at one end of the core, as observed in all such NMR and crystal structures to date. These crystal and docked structures revealed that the chromophore of MM41 is bound slightly asymmetrically onto the terminal G-quartet. Consequently, although three out of four of the substituent chains are each well positioned at the mouth of a G4 groove, the fourth is not. This is due to the limited surface area of the naphthalene diimide chromophore, so that the fourth side chain cannot make effective contacts with a G4 groove and is oriented away from the G4 surface (Figure 1b), consequently, its contribution to overall binding is minimal. We hypothesized that a naphthalene diimide with three substituents would bind with similar affinity and has the advantage of lower molecular weight and reduced overall cationic charge. CM03 (Figure 1c) was therefore conceived and is the subject of the studies reported here. Docking with MM41 and CM03 reveals that the poses for the resulting G4 complexes are similar, even though the CM03 side chains can access only three grooves, while the MM41 targets all four. CM03 is predicted to have each side chain positioned at the mouth of a quadruplex groove (Figure 1d). The aromatic chromophore is positioned slightly off-center because the side chains are not long enough to interact symmetrically in each groove. The two morpholino side chains serve to maximize the binding onto the G-quartet platform.

The synthetic approach to the trisubstituted series adapts previously published procedures to simplify purification and increase yields of both intermediates and final compounds (Scheme 1). 5,5-Dimethyl-1,3-dibromohydantoin was used for the regioselective bromination of the starting material, enabling more efficient and convenient purification. The separation of final products was achieved using column chromatography, giving a 26% overall yield for CM03. It has been formulated as a highly stable mixed chloride/formate salt (pH 6.9), freely soluble in water and saline (>10 mg/mL).

Scheme 1. Synthesis of Compound CM03 (4)[a]

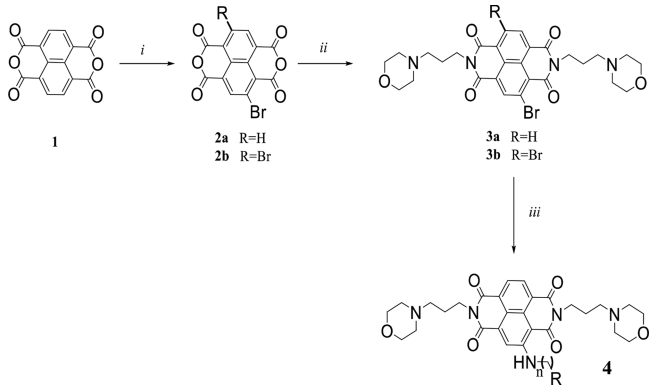

[a](i) 5,5-Dimethyl-1,3-dibromohydantoin, H_2SO_4, 80° C, 72 h; (ii) 3-morpholinopropylamine, acetic acid, microwave, 130 °C, 25 min (The intermediate **3b** was not isolated); (iii) amine, NMP, microwave, 125 °C, 30 min. For CM03, n = 2, R = pyrrolidino. The overall yield of the synthesis for steps i to iii (compound **4**: CM03) was 26%. The yield for steps i and ii (from compound **1** to compound **3a**) was 35%; the yield for final step (iii) (compound **3a** to compound **4** (CM03)) was 75%.

CM03 Shows in Vitro G4 Binding Together with Selective and Potent Antiproliferative Activity. CM03 and MM41 were evaluated for their ability to stabilize G4 binding by means of a fluorescence resonance energy transfer (FRET) protocol using a FAM/TAMRA donor/acceptor combination to measure the temperature (T_m) of the helix–coil transition on gradual heating. A human telomeric G4

DOI: 10.1021/acs.jmedchem.7b01781
J. Med. Chem. 2018, 61, 2500–2517

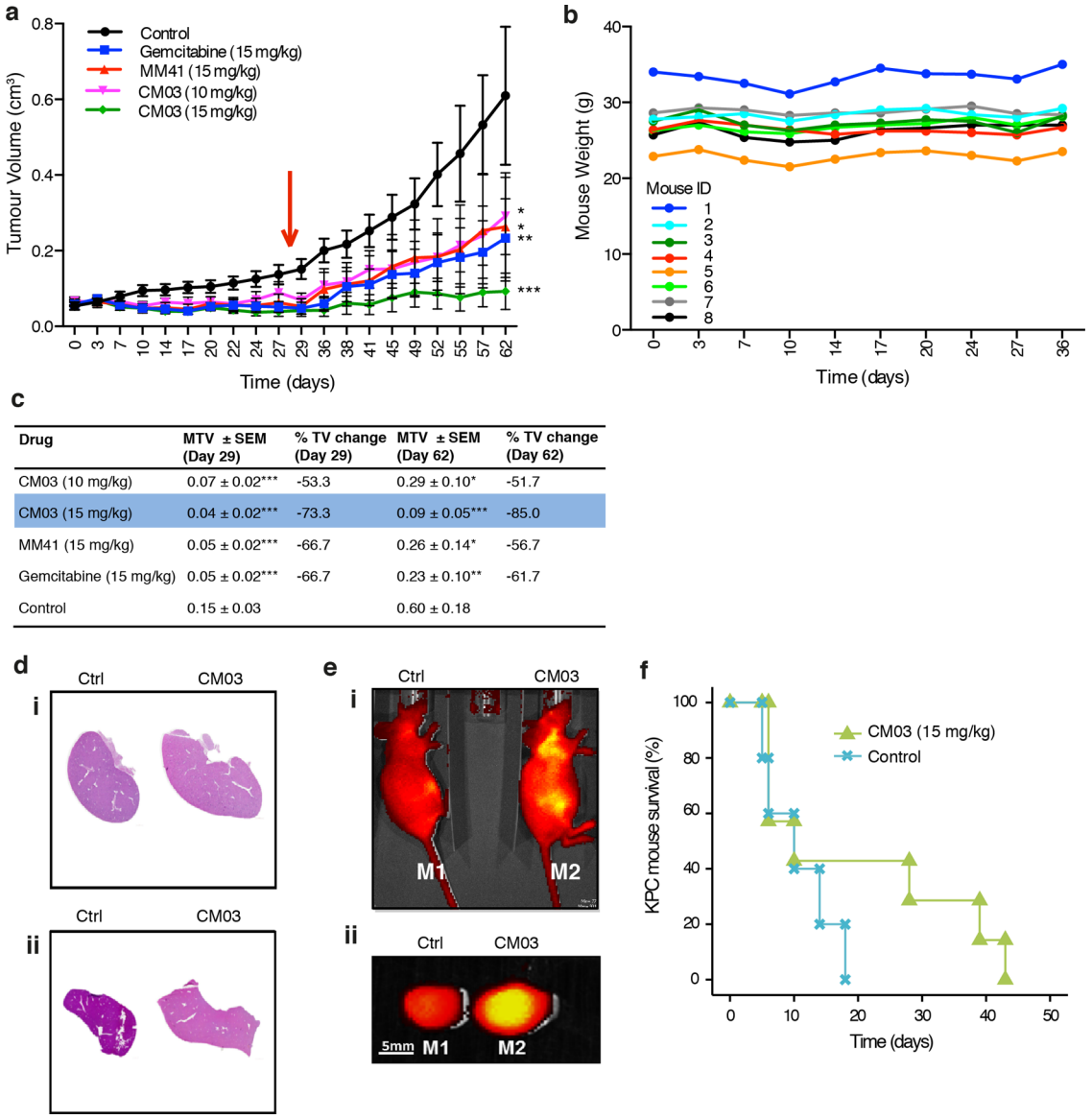

Drug	MTV ± SEM (Day 29)	% TV change (Day 29)	MTV ± SEM (Day 62)	% TV change (Day 62)
CM03 (10 mg/kg)	0.07 ± 0.02***	-53.3	0.29 ± 0.10*	-51.7
CM03 (15 mg/kg)	0.04 ± 0.02***	-73.3	0.09 ± 0.05***	-85.0
MM41 (15 mg/kg)	0.05 ± 0.02***	-66.7	0.26 ± 0.14*	-56.7
Gemcitabine (15 mg/kg)	0.05 ± 0.02***	-66.7	0.23 ± 0.10**	-61.7
Control	0.15 ± 0.03		0.60 ± 0.18	

Figure 2. CM03 treatment reduces tumor volume in a MIA PaCa-2 xenograft model of PDAC. (a) Plot showing the tumor volume of MIA PaCa-2 xenografts treated with CM03, MM41, gemcitabine, or saline (control) over 62 days. There are eight CD-1 mice per condition and dosing for all cohorts was stopped on day 28, shown by the red arrow. Standard error of the mean (SEM) is indicated for all growth curves for each tumor volume. * $p < 0.05$, ** $p < 0.01$, *** $p < 0.001$ (Student t test). (b) A plot of weight for the eight mice in the 15 mg/kg CM03 cohort of this xenograft experiment, for the first 40 days of the experiment. (c) Table showing changes in tumor volume (TV), in cm^3, relative to the control cohort at the selected three time points (MTV represents mean tumor volume). Statistical analysis between the average tumor volume of treated versus control mice cohorts at the given time points was performed using the Student t test * $p < 0.05$, ** $p < 0.01$, *** $p < 0.001$. (d) Sections of hematoxylin and eosin-stained organ tissue, taken from animals at the termination of the xenograft experiment. In each case, images from a single animal are shown. No differences between animals in a cohort were observed. Sections through (i) kidneys and (ii) livers taken from a control (untreated) and a CM03-treated mouse. (e) (i) IVIS images of a saline (control) untreated mouse and a 10 mg/kg CM03 treated mouse with tumors on their flank, 4 h after administration; (ii) IVIS images of the excised tumor from each animal (untreated control and 10 mg/kg CM03 treated) 4 h after administration. (f) Kaplan–Meier plot showing survival of PDAC-bearing KPC mice post onset of treatment (CM03, $n = 7$, control, $n = 5$, Mann–Whitney, $p = 0.217$).

sequence (F21T), together with promoter G4 sequences (from the *HSP90*, *BCL-2*, and *KRAS* genes), and a duplex control (T loop) were screened against the two compounds (Figure 1e). CM03 shows a consistent pattern of ~2-fold (range 1.98–2.25) lower melting stabilization temperature (ΔT_m) compared to MM41 for all tested G4s. The pattern of differences in ΔT_m values between individual G4s is closely similar between the two compounds. Duplex DNA stabilization is significantly reduced for CM03 compared to MM41.

Quantitative binding estimates as K_D values were obtained from fluorescence anisotropy titrations (MM41) and direct fluorescence titrations (CM03). The DNA human telomeric G4 sequence 5′-d(GGGTTAGGGTTAGGGTTAGGG)-3′ was used to enable direct comparisons to be made with the modeling studies. Both compounds bind with nanomolar affinity to this DNA G4, with a ~3-fold difference between MM41 (20 ± 2 nM) and CM03 (67 ± 4 nM).

Compounds were screened with a 96 h SRB (sulforhodamine B) assay for their antiproliferative activity in a panel of human

DOI: 10.1021/acs.jmedchem.7b01781
J. Med. Chem. 2018, 61, 2500–2517

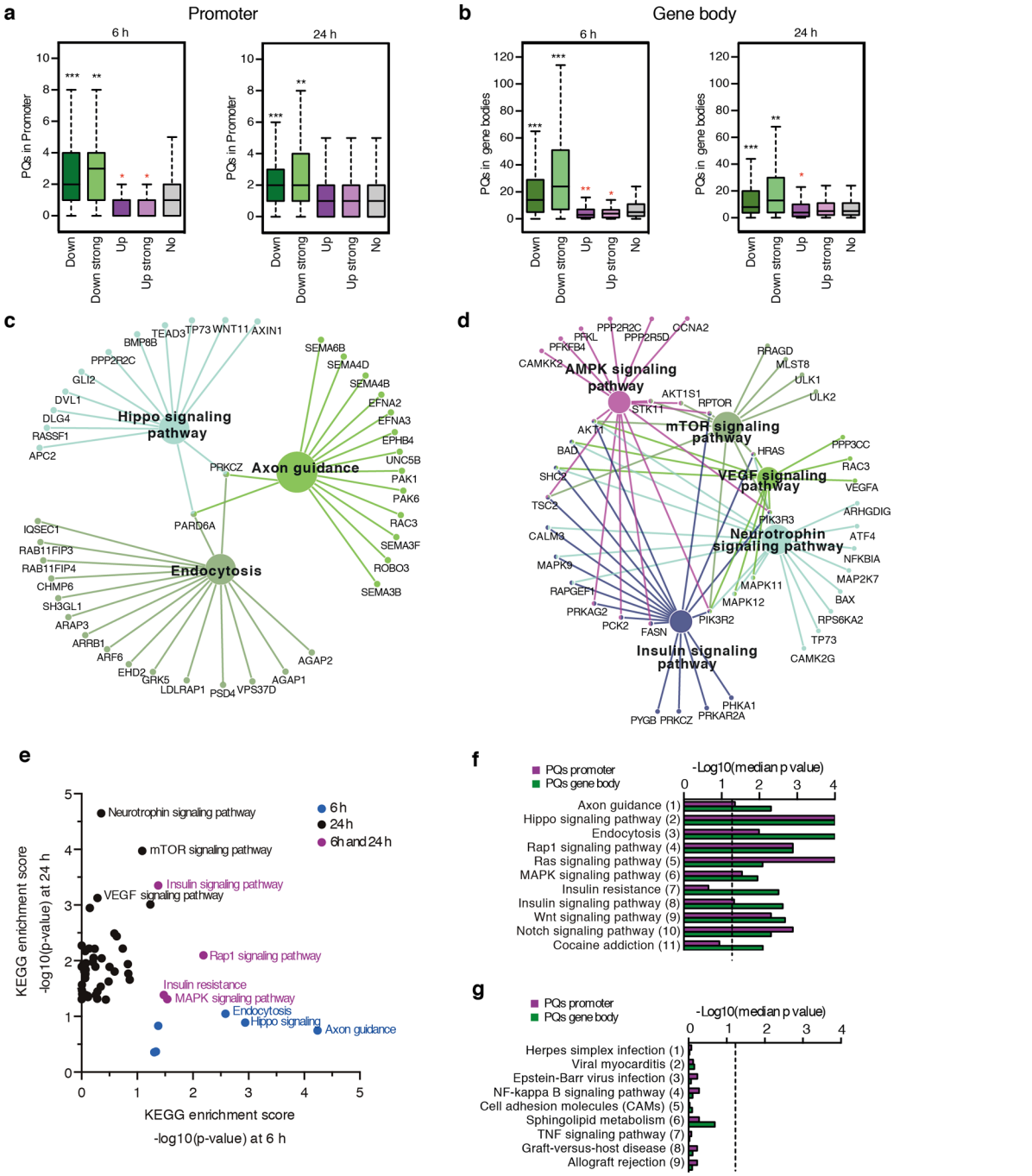

Figure 3. Differentially down-regulated genes common to both PANC-1 and MIA PaCa-2 are enriched in PQs after treatment with 400 nM CM03. (a,b) MIA PaCa-2 and PANC-1 cells were treated with 400 nM CM03 for 6 and 24 h and mRNA extracted for analysis by RNA-Seq. Genes were split into four subgroups according to their fold change upon CM03 treatment versus untreated: Down (Log_2 FC < 0.5, FDR < 0.1), Up (Log_2 FC > 0.5, FDR < 0.1), Down strong (Log_2 FC ≤ 1.0, FDR < 0.05) and Up strong (Log_2 FC ≥ 1.0, FDR < 0.05) and analyzed for PQs occurrence in both (a) promoter (100 bp downstream and 2 kb upstream of the TSS) and (b) gene bodies (exons and introns). See Supporting Information, Table 3 for median and IQR for box and whisker plots. Significance between differentially deregulated gene sets was calculated using the Wilcox statistical test via R software. *$p < 0.05$, ** $p < 1 \times 10^{-10}$, *** $p < 1 \times 10^{-25}$. PQs mean number is significantly lower (red asterisks) or higher (black asterisks) than the no differential expression group (NO). (c,d) enriched KEGG pathways ($p < 0.05$ with Bonferroni correction) and associated down-regulated genes (Log_2 FC < 0.5, FDR < 0.1) common to both PANC-1 and MIA PaCa-2 cell lines after (c) 6 h and (d) 24 h CM03 treatment using the ClueGO Cytoscape App. (e) Scatter plot of significant down-regulated KEGG pathways (p-EASE ≤ 0.05) upon 6 and 24 h CM03 treatment. (f,g) Common (f) down-regulated KEGG pathways after 6 h CM03 treatment are also enriched in promoter and gene body PQs compared to (g) common-up regulated KEGG pathways at 6 h. The significance threshold of 0.05 is represented by the dotted line on the graph.

cancer cell lines comprising lung adenocarcinoma (A549), breast adenocarcinoma (MCF7), and PDAC (MIA PaCa-2 and PANC-1) cell lines, as well as a fetal lung fibroblast-like nononcogenic control cell line (WI-38) (Figure 1f). Both compounds show highly potent growth inhibition activity, particularly for the lung and pancreatic cancer cell lines, which are responsive at low nM concentrations. The responses are highly cell-line-dependent; CM03 shows >20-fold selectivity for

DOI: 10.1021/acs.jmedchem.7b01781
J. Med. Chem. 2018, 61, 2500−2517

MIA PaCa-2 compared to MCF-7 cells. CM03 also shows greater selectivity than MM41 relative to the nononcogenic control fibroblasts (e.g., ~170-fold vs ~21-fold for MIA PaCa-2 cells compared to WI-38 cells for CM03 vs MM41, respectively). CM03 was further examined in additional pancreatic adenocarcinoma cell lines (CAPAN-1 and BX-PC3) and again showed low nM activity (IC_{50} 16 ± 4 and 19 ± 4 nM, respectively). Gemcitabine is also active in these lines at low nanomolar levels, although less so in MIA PaCa-2 (IC_{50} 19 ± 5 nM) and more so in BX-PC3 cells (6 ± 2 nM). Taken together, these results show that CM03 has very potent growth inhibitory activity in cancer versus "normal" cells, particularly for PDAC cells.

CM03 Has in Vivo Antitumor Activity. To determine if the in vitro activity of CM03 was paralleled in vivo, we explored the activity of CM03 in a mouse xenograft model of PDAC. We have previously reported that the maximum tolerated dosage (MTD) for intravenous (IV) administration of MM41 is 25 mg/kg.[33] CM03 was well tolerated, up to a dosage of 45−50 mg/kg, as judged by a dose-escalation MTD study. A therapeutic schedule of two CM03 intravenous (IV) doses was explored using a subcutaneous MIA PaCa-2 pancreatic tumor xenograft model derived from the human cell line used in the cell growth inhibition studies. A group size of eight CD-1 nude mice was used, and dosing was conducted at 10 and 15 mg/kg, each twice weekly, over a period of 4 weeks (28 days: 8 doses). Two further groups were given either MM41 or gemcitabine at 15 mg/kg and received the same dose regimen. Over the course of the experiment, CM03 showed a dose-dependent antitumor response. At the conclusion of dosing on day 28, all four therapy groups showed significant tumor growth inhibition compared to the vehicle control group ($p < 0.001$) (Figure 2a,c), but notably 15 mg/kg CM03 resulted in the highest mean decrease in tumor volume (MTV) (−73%). From day 28 onward, while all treatment groups also showed significant reduction in MTV compared to the control ($p < 0.05$), the 15 mg/kg CM03 cohort consistently showed the greatest therapeutic effect and no tumor regrowth was observed. Five out of the eight animals had tumor volumes that shrank to <0.05 cm^3 by day 62. No body weight reduction (Figure 2b) or adverse effects such as tumor ulceration were observed in this group at any time during the study. Histopathological analysis of vital organs from control and CM03-treated animals sacrificed at the end of the experiments also showed no sign of organ damage (Figure 2d). IVIS imaging of treated mice was performed by taking account of the intrinsic fluorescence of CM03. This showed significant accumulation of CM03 in the tumor xenograft on the flank of the animal (Figure 2e). Thus, in contrast to MM41 and gemcitabine, the higher-dose CM03 treatment results in a statistically significant ($p < 0.001$) antitumor effect, which persisted long after dosing had ceased, up to the termination of the xenograft experiment (62 days).

We also tested the higher dose of CM03 in a genetically engineered mouse model of PDAC. The KPC (*Pdx1-Cre*; *LSL-Kras*$^{G12D/+}$; *LSL-Trp53*$^{R172H/+}$) mouse model is commonly used for preclinical PDAC cancer studies as it develops tumors that exhibit many of the genetic and pathological features of the human disease, including resistance to chemotherapy.[34] Mice with late-stage disease, characterized by swollen abdomen, loss of body conditioning, and palpable tumor, were treated with CM03 intraperitoneally (ip) using the 15 mg/kg twice weekly dosing regimen employed for the xenografts. While the median survival between treated and untreated animals is similar, we note that 3/7 mice survived much longer than all of the untreated animals with two surviving more than twice as long (Figure 2f).

CM03 Induces Down-Regulation of Genes Enriched in G4s. CM03 is a potent G4 ligand, as shown by the FRET and quantitative binding experiments reported here. We therefore reasoned that the potent CM03 antiproliferative activity on PDAC cells could be mediated through a G4-targeting mechanism. To test this hypothesis, we determined whether transcriptome changes upon early CM03 treatment were correlated with G4 presence in promoters and/or gene bodies. Two PDAC cell lines, PANC-1 and MIA PaCa-2 (both with activating KRAS mutations), were treated for 6 or 24 h with 400 nM CM03 (1/10 of the calculated GI_{50} at 24 h, Supporting Information, Figure 1a), RNA was harvested and gene expression levels analyzed by RNA-Seq. The time and dose of CM03 treatment were selected to reveal initial but robust mRNA changes while minimizing chronic effects due to cell toxicity. In both cell lines, the number of genes with altered expression (as defined by >0.5 increase in Log 2 of fold change [Log_2 FC], or < −0.5 decrease; false discovery rate [FDR] < 0.1) increased with duration of CM03 treatment. In PANC-1 cells 2165 genes at 6 h and 3977 genes at 24 h were seen to change, while in MIA PaCa-2 cells, 5306 genes changed at 6 h and 5477 genes at 24 h compared to untreated controls (Supporting Information, Table 1). Suggestive of a common mechanism of action of CM03, the differentially expressed genes were well correlated between the two cell lines at both treatment times (6 h, $r = 0.511$; 24 h, $r = 0.518$) (Supporting Information, Figure 1b−h) with 13044 expressed genes in common (Supporting Information, Table 2) and a high number of genes changed in both cell lines (1185 genes at 6 h, 1917 genes at 24 h). Remarkably, the differentially down-regulated gene set (considering each cell line individually or combined) was significantly enriched ($p < 1 \times 10^{-10}$) for putative G-quadruplexes (PQs), as defined by the $G_{\geq 3}N_{1-7}G_{\geq 3+}N_{1-7}G_{3\geq}N_{1-7}G_{\geq 3}$ consensus sequence,[35,36] in promoters and gene bodies at both 6 and 24 h treatments compared to up-regulated or unaltered genes (cell lines combined, Figure 3a,b; cell lines considered individually, Supporting Information, Figures 2a,b and 3a,b). This association was more marked for genes that were down-regulated to the greatest extent by CM03 (Log_2 FC ≤ 1.0, FDR < 0.05) after 6 h treatment (down strong > down, ratio of means) (Supporting Information, Table 3). To validate that the targeting of G4-containing genes is not a general feature of antiproliferative agents, we also examined the effects of the first-line therapeutic agent for PDAC, gemcitabine,[37] a potent antiproliferative DNA synthesis inhibitor whose mechanism of action is G4-independent and which remains a standard therapy option in advanced PDAC. Both cell lines were treated with a range of gemcitabine concentrations (Supporting Information, Figure 4, Table 4) for 6 or 24 h. Crucially, no significant PQ enrichment was observed for the down-regulated genes in any gemcitabine condition (Supporting Information, Figures 2c,d and 3c,d; 300 nM gemcitabine is shown as an example)). These results strongly support the hypothesis that CM03 specifically targets G4-bearing genes and represses their expression.

To gain insights into possible gene types and pathways targeted by CM03, we performed a KEGG gene enrichment pathway analysis of the common down-regulated genes. This revealed a total of 11 and 46 significant pathways (p-EASE ≤

DOI: 10.1021/acs.jmedchem.7b01781
J. Med. Chem. 2018, 61, 2500−2517

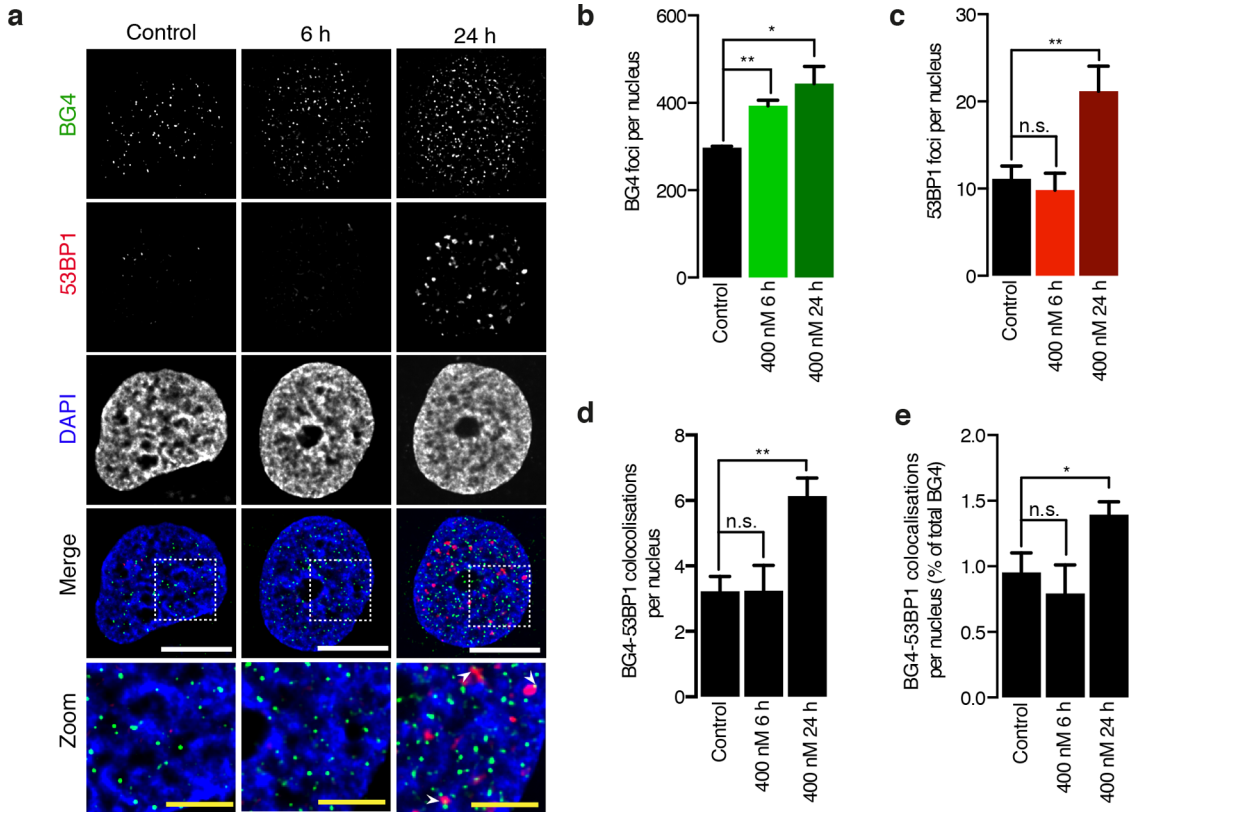

Figure 4. CM03 treatment induces DNA damage and increases the presence of nuclear G4. (a) Following 6 and 24 h treatment with 400 nM CM03, PANC-1 cells were fixed with paraformaldehyde and stained with antibodies against G4s (BG4, green) and the DNA damage marker 53BP1 (red). *Z*-Stack images (11 μm × 0.3 μm spacing) were captured using a Nikon wide-field microscope and deconvolved using Hugyens Professional software. The central slice of the *Z*-stack is shown in the representative images. White scale bar is 10 μm. Zoom panel represents increased magnification of the highlighted section of the nucleus (dotted square) in the Merge panel. Yellow scale bar is 2.5 μm. Detection and co-localization between BG4 and 53BP1 foci (white arrows) were performed using a custom protocol in the ICY software, which utilizes the spot detector and co-localization studio plugins with the wavelet and Ripley's K functions (see Methods). (b–e) The graphs show the mean number of (b) BG4 foci, (c) 53BP1 foci, (d) BG4-53BP1 co-localizations, or (e) percentage of total BG4 co-localizing with 53BP1 per nucleus with the standard deviation from three biological replicates. A two-tailed Student's *t* test was used to determine statistical significance across each condition ($p < 0.05$ = *, $p < 0.01$ = **; n.s. = not significant). Each biological replicate represents 50–100 nuclei.

0.05) after 6 and 24 h CM03 treatment, respectively. Many of these pathways, or genes within them, have been previously associated with PDAC (Figure 3c,d, Supporting Information, Figures 5, 6; Tables 5, 6) such as axon guidance (14 genes, $p = 5.75 \times 10^{-5}$),[7] the hippo signaling pathway (13 genes, $p = 1.15 \times 10^{-3}$)[38] at 6 h, mTOR (12 genes, $p = 1.07 \times 10^{-4}$)[39] and VEGF signaling pathways (11 genes, $p = 7.45 \times 10^{-4}$)[40] after 24 h and insulin resistance,[41] and Rap1 and MAPK signaling pathways across both time points[40] (Figure 3e). This contrasts with the pattern of the common up-regulated genes at 6 and 24 h (9 and 10 significant pathways, respectively) after CM03 treatment, with particular enrichment in cellular matrix adhesion and major histocompatibility complex proteins pathways (Supporting Information, Figure 7a). As anticipated, 300 nM gemcitabine treatment affected strikingly different KEGG pathways compared to CM03 (Supporting Information, Table 7). The most significant down-regulated gemcitabine pathways (for both cell lines) were cell cycle after 6 h and ribosome-associated pathways after 24 h, which is consistent with its known mechanism of action in inhibiting DNA synthesis, cell cycle progression, and global translation.[37] This contrasts with known pathways seen to be up-regulated after gemcitabine treatment which includes the NF-Kappa B signaling pathway ($p = 1.61 \times 10^{-6}$) for PANC-1[42] and the Fanconi anemia pathway ($p = 6.46 \times 10^{-6}$) for MIA PaCa-2.[43] It is notable that PQs in promoters and gene bodies are highly enriched within down-regulated KEGG gene pathways after CM03 treatment (Figures 3f, Supporting Information, Figure 7b) compared to random sampling across the expressed genes or to up-regulated genes (Figure 3g and Supporting Information, Figure 7c). Overall, these results robustly support our contention that CM03 specifically targets critical pathways that lead to pancreatic cell death via the inhibition of expression gene sets harboring a G4 structure.

CM03 Treatment Results in an Increase in BG4 Foci and DNA Damage. Because many established G4-stabilizing ligands induce transcription and replication-coupled DNA damage in the vicinity of G4-forming sequences,[44] we investigated whether CM03 treatment affects cellular G4 occurrence and/or induces a DNA damage response. To do this, we treated asynchronous PANC-1 cells with CM03 and performed immunofluorescence staining using the G4-specific antibody BG4[18] and an antibody against the DNA damage and double-strand break (DSB) marker 53BP1[45] followed by 3D image construction and analysis. As predicted, 400 nM CM03 treatment resulted in a time-dependent significant ($p < 0.05$) increase in the number of nuclear BG4 foci (Figure 4a,b) (393 ± 13 at 6 h and 444 ± 39 BG4 foci at 24 h) compared to

DOI: 10.1021/acs.jmedchem.7b01781
J. Med. Chem. 2018, 61, 2500–2517

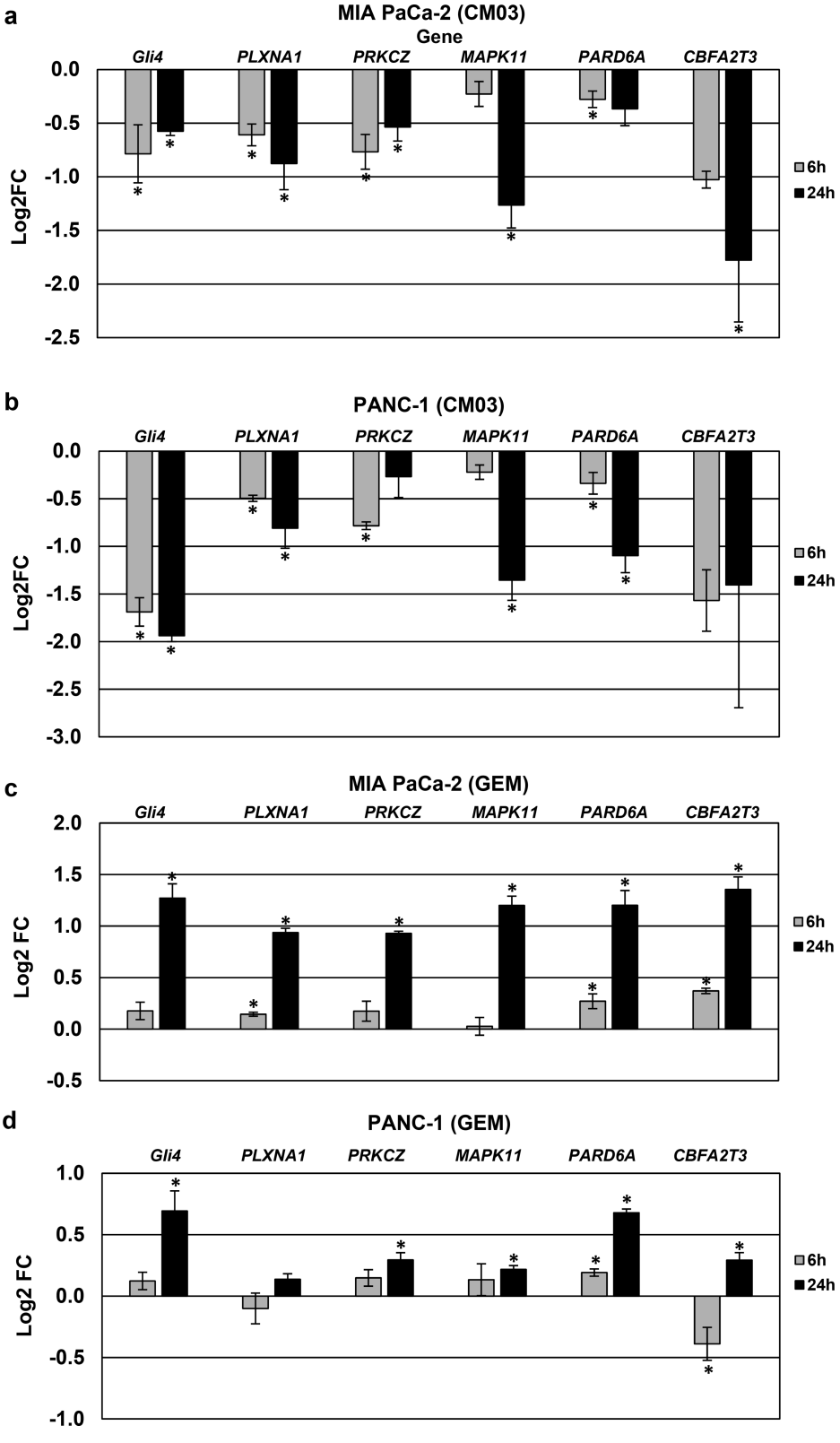

Figure 5. Validation of mRNA down regulation by qRT-PCR for a subset of down-regulated genes, selected from RNA-Seq experiments. (a–d) MIA PaCa-2 and PANC-1 cells were treated (a and b) with 400 nM CM03 and (c and d) with 400 nM gemcitabine, all for 6 and 24 h. Total mRNA was extracted, reverse transcribed into cDNA, and then qRT-PCR was performed. The C_t values were normalized to the genomic mean of three housekeeping genes (*ACTB*, *GAPDH*, and *TUBB*), and the relative gene expression was determined using the Livak method, $2^{-\Delta\Delta Ct}$. The log-fold expression changes (Log_2 FC) for each gene are shown relative to vehicle-treated controls (PBS for CM03 and DMSO for gemcitabine). Student's *t* test along with $2^{-\Delta Ct}$ values were used to determine the statistical significance of the observed changes, which are the mean of in each case at least three determinations. Those genes with changes in expression with $p < 0.05$ have been marked *.

DOI: 10.1021/acs.jmedchem.7b01781
J. Med. Chem. 2018, 61, 2500–2517

controls (297 ± 3 BG4 foci). This further confirms that CM03 has a direct action at G4 sites to increase G4 stabilization. Consistent with the capability of unresolved endogenous genomic G4 sites[46] and small molecule-stabilized G4s to obstruct DNA replication,[44] a 2-fold increase in the number of 53BP1 foci was only apparent after 24 h treatment with CM03 (11 ± 2 compared to 21 ± 3 53BP1 foci) (Figure 4a,c). To determine if CM03 induced DNA damage directly at G4 sites, we calculated the extent of co-localization between BG4 and 53BP1 foci using object-based image co-localization analysis. While the percentage of co-localization between BG4 and 53BP1 reproducibly increased by 50% after 24 h 400 nM CM03 treatment (Figure 4d), only 1.4% of total BG4 foci per nucleus were associated with DNA damage foci (Figure 4e). Nonetheless, our data strongly suggests CM03 stabilizes G4 structures leading to an accumulation of nuclear G4 foci accompanied by the induction of DNA damage and replicative stress.

DISCUSSION AND CONCLUSIONS

While PDAC is predominantly (>95%) driven by oncogenic KRAS,[40] the development of more targeted therapies against KRAS and other core PDAC associated pro-survival pathways including: Ras-Raf-MEK-ERK and PI3K-AKt-mTOR have proved futile owing to the highly mutagenic nature of the disease[5−8] and the ability of PDAC cells to rapidly switch between phenotypic states, resulting in the evasion of therapy.[47] As novel alternative strategies for intervention in PDAC are urgently required, the targeting of G4s with small molecules has been proposed as an innovative method for selective cancer therapy.[14] This is supported by recent G4-ChIP-seq and G4-IF studies identifying an increased abundance of G4s in cancer versus normal cells, as well as G4 structure enrichment at oncogenes.[16] We have recently reported that the G4 ligand MM41[33] reduces tumor volume by ∼80% in a PDAC xenograft model. MM41 binds strongly to the G4s in the down-regulated genes *KRAS* and *BCL-2*, resulting in cell apoptosis, and suggested that G4 ligand treatment is potentially a highly effective method for targeting PDAC. MM41 is a suboptimal drug candidate due to its higher molecular weight and four positive charges.[32] We present here CM03 as an improved rationally designed derivative of MM41 and as a novel lead candidate compound for potential PDAC therapy in humans. CM03 has comparable affinity for a human telomeric G4 to the tetra-substituent compound MM41, indicating that the fourth side chain and increased cationic charge on MM41 does not make a major contribution to affinity. Although affinities for CM03 or MM41 binding to (a single) G4 in vitro may be difficult to directly relate to cell growth inhibitory properties, CM03 is as potent in cells as MM41. Both compounds show good selectivity for cancer cell lines (especially pancreatic) over "normal" nononcogenic fibroblasts, but CM03 shows >4-fold less activity toward the WI-38 cell line. This enhanced selectivity is also apparent in vivo, where CM03 has a higher level of tolerability (higher MTD) compared to MM41. This suggests that the fourth side chain of MM41 may add to off-target toxicity burden; however, neither MM41 nor CM03 show significant hERG liabilities (unpublished data), a common indicator of cardiotoxic effects. The antitumor activity of CM03 results in sustained tumor growth arrest, which continues long after dosing is ceased and compares favorably with the growth delay typically seen with experimental antitumor agents.[25] The increased animal survival in a subset of the autochthonous KPC mice to CM03 suggests that CM03 may be able to effectively penetrate the tumor stroma microenvironment characteristic of human PDAC.

The RNA-seq data revealed that treatment with CM03 resulted in a striking global differential down-regulation of genes containing putative G4s (PQs), which occurred as early as 6 h after treatment. We have performed RT-qPCR on a small set of the genes down-regulated by CM03 (Figure 5a, b). The results confirm the RNA-seq analyses: that these PDAC-pathway genes are transcriptionally down-regulated in both cell lines and that they are not significantly affected by gemcitabine (Figure 5c,d). The RNA-seq results are consistent with the hypothesis that G4 ligands can alter gene expression when PQs are targets in individual genes.[23] Previously, global G4-motif specific changes in the transcriptome with bisquinolinium compounds in HeLa cells have been reported using microarray analysis.[48] However, our work represents the first comprehensive analysis using state-of-the-art RNA-seq methodology. This is the first demonstration that a G4-binding small molecule produces global down-regulation of G4-containing genes in human cancer cell lines, in striking comparison with a non-G4 targeting drug, the modified nucleoside gemcitabine. Moreover, as we identify G4 effects at much earlier times and smaller doses than earlier studies, this further demonstrates that CM03 is a bona fide G4 ligand in cells and, by implication, in vivo as well. The observed transcriptional effects of CM03 also align with the hypothesis that down-regulation of gene expression is mediated through ligand-stabilized G4s, causing for example steric hindrance and inhibition of RNA pol II in the transcription bubble (reviewed in ref 23). The observations that transcriptional effects are closely aligned in two PDAC cell lines, independently sequenced, gives added confidence to these conclusions.

KEGG pathway analysis shows that CM03 targets 42 pathways, many of which are key to PDAC development and maintenance. The most significant down-regulated pathways after 6 h were the hippo signaling, axon guidance, and endocytosis pathways, which are all deregulated in PDAC.

Hippo signaling acts through the core transcription factors, YAP and TAZ. In PDAC, both YAP and TAZ are overexpressed and are essential for neoplastic progression.[49] YAP/TAZ also contributes to PDAC resistance to therapeutic approaches directly targeting mutant KRAS.[50,51] Notably, CM03 down-regulates three prime effectors of YAP function, TEAD2 and -4 (MIA PaCa-2 only) and TEAD3 (both cell lines) at 6 h. As TEAD 2/4 are oncogenic in many cancers,[52] CM03 may be suitable as a global cancer therapeutic agent. CM03 also down-regulates the oncogenic Gli transcription factors Gli2/4, downstream of TEAD and highly up regulated in PDAC.[6] As Gli2 is essential for KRAS-driven oncogenesis in vivo[53] and plays a role in PDAC resistance to both gemcitabine[54] and BET inhibitors,[55] this suggests CM03 may have a novel therapeutic potential.

For the axon guidance pathway, key PQs-containing genes down-regulated by CM03 are *PAK1*,[56] *ROBO3*,[57] and *PLXNA1*,[58] all of which are highly overexpressed in PDAC. While axon guidance is a neurodevelopmental process, many axon guidance genes are deregulated in many cancers, including PDAC, and contribute to metastasis and tumor growth.[7,59] *PAK1* mediates pancreatic cancer cell migration, growth, promotes epithelial to mesenchymal transition (EMT), and is crucial in conferring gemcitabine resistance.[56] Expression of the SLIT3 receptor, ROBO3, increases with PDAC clinical grade and is anticorrelated with patient survival.[7] As ROBO3

DOI: 10.1021/acs.jmedchem.7b01781
J. Med. Chem. 2018, 61, 2500−2517

Table 1. RNA-Seq Expression Data for a Select Set of Down-Regulated Genes after CM03 Treatment[a]

	Log_2 FC (6 h)		Log_2 FC (24 h)			no. of PQs	
gene symbol	PANC-1	MIA PaCa-2	PANC-1	MIA PaCa-2	gene function	exons and introns	promoter
AKT1	−0.18	−0.20	−1.04	−0.98	key protein kinase for (the AKT-mTOR signaling pathway: involved in metabolism, proliferation, cell survival, growth, and angiogenesis	44	2
AKT1S1	−0.11	−0.54	−0.83	−1.09	subunit of mTORC1: regulates cell growth and survival in response to nutrient and hormone signals	5	2
ARF6[c]	−0.74	−0.89	−0.69	−0.54	RAS GTPase, protein trafficking, regulates endocytic recycling and cytoskeleton remodelling, noncanonical EGRF, and hedgehog signaling pathways	1	3
CBFA2T3[b,c]	−2.18	−2.74	−2.25	−2.86	transcription regulator, HDAC pathways	96	4
CTBP1[c]	−0.66	−0.52	−0.98	−1.17	transcriptional corepressor: oncogenic, required for PAK1-dependent macropinocytosis	47	3
FASN	−0.73	−0.06	−0.70	−0.54	fatty acid synthase	40	4
GLI1	0.03	−0.61	−0.57	−0.64	transcriptional activator, mediates hedgehog signaling	15	4
GLI2	−0.67	−1.17	0.38	−1.24	KRAS-driven oncogenesis, gemcitabine and BET inhibitor resistance, effector of TEAD proteins, transcription regulator in hedgehog pathway	71	0
GLI4[c]	−1.26	−1.71	−1.71	−1.85	up-regulated in PDAC, effector of TEAD proteins	11	0
IGF2	−1.15	−2.72	−1.53	0.72	insulin-like growth factor	34	8
IQSEC1[c]	−0.86	−1.11	−0.50	−0.53	guanine nucleotide exchange factor for ARF1 and ARF6	82	5
MAPK11	−0.38	−0.53	−1.60	−2.56	essential effector kinase of p38 MAPK pathway	18	6
MAPK12	−0.75	−0.47	−1.44	−1.23	essential effector kinase of p38 MAPK pathway	18	6
MAPK9	−0.28	−0.09	−0.75	−0.60	essential effector kinase of JNK signaling pathway	10	3
mLST8[c]	−0.54	−0.76	−1.72	−1.28	subunit of both mTORC1 and mTORC2	8	1
PAK1[c]	−0.54	−0.59	−1.11	−1.13	protein kinase: involved in cancer cell migration and growth, macropinocytosis, gemcitabine resistance	14	3
PARD6A[b,c]	−0.63	−0.83	−1.41	−1.40	tumour cell motility and metastatic potential	3	3
PCK2	−0.01	0.26	−0.56	−0.82	catalytic enzyme required for rate limiting step in gluconeogenesis	6	0
PFKFB4[c]	−0.57	−1.02	−0.74	−0.93	glycolysis: synthesis and degradation of fructose 2,6-bisphosphate	10	2
PFKL	−0 21	0.00	−0.98	−1.18	catalytic enzyme for first step of glycolysis	34	4
PIK3R2	−0.45	−0.55	−0.88	−1.14	regulatory subunit of PI3K	13	0
PIK3R3	−0.16	−0.28	−0.54	−1.47	binds to activated PI3K and regulates kinase activity	2	1
PLXNA1[b,c]	−0.84	−0.98	−1.50	−1.56	receptor for class 3 semaphorins: involved in cancer invasion, migration, and growth	54	3
PRDM16[b,c]	−2.40	−2.73	−314	−3.39	transcription regulator: TGF8, SMAD pathways	260	5
PRKCZ[c]	−1.44	−1.87	−1.23	−2.01	cell polarity: PI3K, MAPK signaling pathway, NF-kappa-beta activation	78	3
ROBO3[c]	−0.75	−0.86	−0.85	−0.53	axon guidance receptor, promoters liver metastasis through Wnt signaling, expression increases with clinical grade of PDAC	19	3
RPTOR[c]	−0.80	−1.41	−0.50	−0 68	scaffold lor recruiting mTORC1 substrates	104	1
SHANK2[b]	−1.65	−1.87	−0.44	−1.96	axon guidance, SRC pathways	203	4
SHC2[c]	−0.52	−0.83	−1.47	−1.96	signaling adapter for insulin and VEGF signaling	41	8
SMO	−0.92	−0.34	−0.82	−1.21	G protein-coupled receptor: transduces hedgehog signaling	12	1
TEAD2	−0.22	−0.65	0.21	−0.91	transcription factor, facilitates YAP interaction with DNA (Hippo pathway)	19	10
TEAD3	−0.59	−1.06	0.07	−0.66	transcription factor, facilitates YAP interaction with DNA (Hippo pathway)	29	7
TEAD4	−0.23	−0.79	−0.47	−0.31	transcription factor, facilitates YAP interaction with DNA (Hippo pathway)	34	6
TP73[b,c]	−1.44	−2.36	−0.99	−1.19	cell cycle, DNA repair regulation	91	5
ULK1	0.19	0.03	−0.81	−0.60	protein kinase autophagy: regulates formation of autophagosomes	38	6

[a] Log_2 FC gene expression changes after 6 and 24 h CM03 treatment, the number of PQs and gene function are shown. Common down-regulated genes are defined as having Log_2 FC < 0.05 and FDR < 0.1 in both cell lines and genes are ranked by the lowest average Log_2 FC. [b] The methylation status of genes has been associated with patient survival (see Discussion). [c] Genes down-regulated (Log_2 FC < 0.05, FDR < 0.1) in both cell lines at 6 and 24 h CM03 treatment.

promotes liver metastasis and tumor growth via Wnt signaling pathway,[59] this again suggests a more general CM03 therapeutic applicability. Likewise, the SEMA3A receptor, PLXNA1, is up-regulated in PDAC and linked with poor patient prognosis due to altered PLXNA1−SEMA3A signaling.[7,58]

PDAC tumors experience hypoxia and nutrient deprivation due to the dense surrounding tissue stroma, thus PDAC heavily relies on endocytosis for scavenging of essential metabolites and receptors/transporters recycling.[60] A key endocytotic gene *ARF6*, a member of the RAS superfamily of small GTPases involved in plasma membrane trafficking, cell motility, cytokinesis, and cholesterol homeostasis,[61] is strikingly down-regulated by CM03 (by 6 h). Mutant KRAS induces ARF6, which acts as an oncogene in PDAC to drive the constitutive activation of the ERK1/2 signaling and downstream effector MYC, to regulate the Warburg effect.[62] ARF6 has many other roles including GLUT1 and CD95 receptor recycling,[61]

DOI: 10.1021/acs.jmedchem.7b01781
J. Med. Chem. 2018, 61, 2500−2517

noncanonical EGRF and Hedgehog (Hh) signaling, and Hh-mediated chemo-resistance.[63] Furthermore, CM03 also targets *IQSEC1*, a guanine nucleotide-exchange factor that is responsible for activating ARF6 and whose down-regulation inhibits PDAC invasion by preventing internalization of E-cadherin from the plasma membrane.[64] Other significant pathways with CM03 down-regulated genes (at 24 h) involved in altered PDAC metabolism include: fatty acid synthesis (oncogene fatty acid synthase (*FASN*)),[60] glycolysis (*PCK2*, *PFKL*, and *PFKFB4*),[65] autophagy (*ULK1*), and macropinocytosis (*PAK1* and *CTBP1*).[66]

Other key genes down-regulated by CM03 (by 6 h) which also impinge on the above pathways include the binding partners Par6 (*PARD6A*) and PRKCZ that are important for tumor cell motility and metastatic potential in PDAC through activation of JAK/STAT signaling pathway.[67] Par6 also binds PRKCi, another atypical protein kinase, which promotes PDAC transformation partly through activation of the Rac1-MEK/ERK signaling pathway.[68] Of note, *PARD6A* knockdown significantly reduces anchorage dependent growth and cell invasion of both PRKCZ and PRKCi nonredundant pathways.[67] The PKCi−Par6 complex also plays an oncogenic role in lung, ovarian, and colon cancer.[68] Together, this suggests that CM03 could be effective in multiple cancer types. Other CM03 down-regulated genes whose DNA methylation status correlates with pancreatic cancer patient survival[69] include *PRDM16* (rank 2), *SHANK2* (rank 31), *CBFA2T3* (rank 4), and *TP73* (rank 20) (at 6 h, Supporting Information, Table 2).

For PDACs driven by mutant KRAS, drug resistance depends on a balance between PI3K/AKT/mTOR and MAPK/ERK pathways and YAP1 and MYC up-regulation.[70] It is striking that CM03 treatment down regulates many elements of this mechanism (see Table 1). For example AKT (*AKT1*), key effectors of mTOR (*RPTOR*, *mLST8*, *AKT1S1*), PI3K pathway (*PIK3R3* and *PIK3R2*) and MAPK proteins (*MAPK9*, *MAPK11*, and *MAPK12*) are down-regulated in both PDAC cell lines by CM03 (by 24 h). In the noncanonical Hh-mediated gemcitabine resistance pathway the transcript levels of *SMO* and *GLI1* are also down-regulated by CM03.[54] Tumor associated macrophages and cancer-associated myofibroblasts in tissue stroma are also key drivers for chemoresistance in PDAC, and it is notable that IGF2 and SHC2 are down-regulated by CM03 as these proteins have been implicated in insulin receptor-mediated chemoresistance.[71] Collectively, these findings clearly demonstrate the ability of CM03 to simultaneously target several fundamental PDAC tumorigenesis mechanisms.

Curiously, while CM03 shows binding affinity to *KRAS* G4s in vitro (Figure 1e), our RNA-SEQ studies show that *KRAS* mRNA expression is unaffected by CM03 treatment in either pancreatic cell line at the times and doses tested (Supporting Information, Table 1). It may be that in a cellular context the *KRAS* G4 is rapidly resolved by unwinding helicases or that G4 binding proteins hinder drug accessibility. Thus, while the *KRAS* G4s may not be the main/initial target of CM03, we cannot assume the accessibility of *KRAS* G4 for CM03 within the native epigenetic environment. Nonetheless, our results suggests that simultaneous targeting of multiple fundamental PDAC pathways (including important KRAS effector and feedback loop signaling pathways and those involved in drug resistance) by G4 stabilization will be an advantageous approach.

CM03 also resulted in the induction of DNA damage in a replication-dependent manner. While the number of BG4 foci increased upon CM03 treatment suggesting increased G4 stabilization, only a small increase in BG4 and 53BP1 co-localization was observed. It is tempting to suggest that CM03 does not cause an increase in damage at G4 sites, however, the dynamics of whether a G4 structure can co-exist with DNA damage response proteins is not well understood or whether G4s persist after DNA damage response and repair have been elicited. In support, many DNA repair pathway proteins are capable of unwinding and destabilizing G4,[72] and a recent study has elucidated the role of PARP3 negatively regulating G4 in order to initiate DNA repair at DSB sites.[73] Hence, by 24 h, the small number of co-localizations could represent an intermediate repair state of DNA at a G4 site.

In summary, we have demonstrated that CM03 is a highly potent G4-binding small molecule, with in vitro cell assays and in vivo models for human PDAC. Treatment with CM03 successfully reduced tumor growth for an extended period in PDAC xenografts and also prolonged survival in the KPC mouse model for this disease at dosage levels that do not cause observable damage to major organs yet enable selective tumor targeting. It is notable that the antitumor effects of CM03 in the xenograft model persisted until the termination of the experiment at day 62 (34 days beyond the end of dosing). This is in striking contrast to the antitumor response to gemcitabine, with tumor regrowth being apparent as soon as dosing was stopped.

Studies with PDAC cell lines suggest that the mechanism of action of CM03 is via the G4-dependent down-regulation of genes in a number of essential pathways associated with PDAC survival, metastasis, and drug resistance, together with the activation of G4 replication-dependent DNA damage. Furthermore, given the good bioavailability of CM03 and its ability to target many oncogenic pathways essential to tumorigenesis in general, we suggest that CM03 has the potential to be used as an effective anticancer therapeutic in a number of other cancers in addition to PDAC. It is tempting to speculate that the selective tumor targeting is associated with G4 binding, and future studies will address this question.

EXPERIMENTAL METHODS

Chemistry. The synthesis and characterization of MM41 (4,9-bis((3-(4-methylpiperazin-1-yl)propyl)amino)-2,7-bis(3-morpholinopropyl)benzo[*lmn*][3,8]phenanthroline-1,3,6,8(2*H*,7*H*)-tetraone: molecular weight 831.08) has been previously reported.[32a] MM41 was analytically pure as shown by LC-MS and NMR methods and was formulated for biological studies as the freely water-soluble formate salt.

The traditional synthetic route to highly substituted naphthalene diimides starts from 1,4,5,8-naphthalene tetracarboxylic dianhydride, which is then reacted with dibromoisocyanuric acid, leading to the mono- and dibromonaphthalene diimide as key intermediates, followed by introduction of the amine chains at the imide and bay positions, in that order. This synthesis results in a complex mixture requiring purification by preparative HPLC at least twice to obtain the desired products in very low yield (less than 10%). The critical aspect of the present synthetic scheme was preparation of the monobrominated naphthalene diimide precursor; this is insoluble, so purification at this stage was not attempted, nor was there any evaluation of the amount of monobromo derivative obtained. Purification can be performed only after the N−N′ imidation reaction due to the aqueous solubility that is imparted by the introduction of the basic morpholino side chains. Instead, the procedure was modified as shown in Scheme 1.

DOI: 10.1021/acs.jmedchem.7b01781
J. Med. Chem. 2018, 61, 2500−2517

All chemicals, reagents, and solvents were purchased from Sigma-Aldrich, Alfa Aesar, Lancaster Synthesis, and Fluorochem (UK) and used without further purification. Solvents were supplied by VWR and Fisher Scientific. Column chromatography was performed using BDH silica gel (BDH 153325P). Chromatography was conducted under medium pressure in glass columns or using a Biotage SP4 instrument in prepacked columns (FLASH Silica columns (40−63 μm, 60 Å)). HPLC analysis was carried out with a Gilson apparatus combining a 322 pump and an Agilent 1100 series detector, using a C18 5 μ (100 mm × 4.6 mm) column (41622271 (W), YMC, Japan) at a flow of 1 mL/min. Preparative HPLC was carried out with a Gilson apparatus combining a 322 pump and a UV/vis-155 detector with detection at 280 nm, using a C18 5 μ (100 mm × 20 mm) column (201022272) (W), YMC, Japan, at a flow of 20 mL/min. Water and methanol with 0.1% formic acid were used as solvents for HPLC. For the purification of compound CM03, the following method was used: 100% aqueous solution for 5 min after injection, then gradually decreased to 60% aqueous solution over 25 min.

*2-Bromo-1,4,5,8-naphthalenetetracarboxylic Acid Dianhydride (**2a**) and 2,6-Dibromo-1,4,5,8-naphthalenetetracarboxylic Acid Dianhydride (**2b**).* Naphthalene dianhydride (**1**, from Sigma-Aldrich) (150 mg, 0.56 mmol) was slurried in sulfuric acid (1.5 mL), and the suspension obtained was stirred for 5 min at room temperature to allow the complete dissolution. 5,5-Dimethyl-1,3-dibromohydantoin (88 mg, 0.308 mmol) was added slowly over a period of 1 h, and the round-bottom flask was tightly stopped to avoid the escape of bromine from the reaction mixture. The solution was stirred at 80 °C for 72 h and then poured onto ice (30 mL). The yellow solid formed was filtered, washed with water (2 × 10 mL), and dried under vacuum, yielding a mixture **2a** and **2b**. No NMR data were obtained due to solubility issues. The resulting mixture was used without further purification in the next step.

*N,N′-Bis(3-(morpholino)propylamino)-2-bromo-1,4,5,8-naphthalenetetracarboxylic Acid Diimide (**3a**).* Compounds **2a** and **2b** (194 mg, 0.56 mmol) were suspended with sonication in glacial acetic acid (1.5 mL) in a microwave reaction vessel. 3-Morpholinopropyalamine (242 mg, 245 μL, 1.68 mmol) was added dropwise to the stirring mixture. The reaction tube was sealed and treated for 30 min at 125 °C in the microwave. The solution was then basified with potassium carbonate and extracted with chloroform (3 × 5 mL). The organic phases were collected, dried over sodium sulfate, and evaporated. The residue obtained was purified through column chromatography using as eluent a CH_2Cl_2/MeOH 96/40 mixture. Yield **3a** (107 mg, 0.18 mmol, 35%). ^{1}H NMR ($CDCl_3$) δ 1.95−1.97 (m, 4H), 2.40−2.43 (m, 8H), 2.52−2.53 (m, 4H), 3.51−3.54 (m, 8H), 4.28−4.33 (q, 4H, *J* = 8 Hz), 8.77 (d, 1H, *J* = 8 Hz), 8.82 (d, 1H, *J* = 7.6 Hz), 8.935 (s, 1H). ^{13}C NMR (100 MHz, $CDCl_3$, TMS) δ 23.31, 23.44, 38.81, 39.11, 52.50, 55.51, 55.45, 65.37, 65.41, 123.97, 125.75, 125.95 (2C), 126.01, 126.84, 128.68, 128.76, 130.73, 131.71, 138.44, 161.17, 161.87, 161.98, 162.56. HRMS (ES^+) calculated $C_{28}H_{33}BrN_4O_6$ $[M + 2H]^+$ 600.1543, found 600.1536.

*2,7-Bis(3-morpholinopropyl)-4-((2-(pyrrolidin-1-yl)ethyl)amino)-benzo[lmn][3,8]phenanthroline-1,3,6,8(2H,7H)-tetraone (Compound **4**: CM03).* Compound **3a** (0.15 g, 0.25 mmol), 1-(2-aminoethyl)pyrrolidine (0.06 mL, 0.51 mmol), and NMP (1 mL) were suspended in a microwave reaction vessel. The reaction tube was sealed and treated for 25 min at 130 °C in the microwave. After having been cooled to room temperature, the solvent was concentrated and the crude mixture was purified by column chromatography, using as eluent a mixture of CH_2Cl_2/MeOH/NH_3 95/5/0.4. Compound **4** was obtained as a red oil (118 mg, 0.186 mmol, 75% yield). ^{1}H NMR (400 MHz, $CDCl_3$, TMS) δ 2.019−2.040 (m, 8H), 2.683−2.782 (m, 12H), 3.195 (t, 4H, *J* = 6.4 Hz), 3.32 (t, 2H, *J* = 6.6 Hz), 3.708 (t, 4H, *J* = 4.8 Hz), 3.764 (t, 4H, *J* = 4.6 Hz), 4.009−4.024 (m, 2H), 4.22 (t, 4H, *J* = 7 Hz), 8.237 (s, 1H), 8.28 (d, 1H, *J* = 7.6 Hz), 8.56 (d, 1H, *J* = 8 Hz), 10.174 (t, 1H, exch D_2O, *J* = 4.2 Hz). ^{13}C NMR (100 MHz, $CDCl_3$) δ 23.3, 23.6, 23.7, 38.2, 38.9, 40.1, 52.6, 52.8, 53.9, 53.9, 55.8 (2C), 65.6, 65.8, 100.7, 119.1, 119.5, 123.5, 124.9, 126.1, 128.0, 129.2, 131.4, 151.8, 162.8, 163.2, 165.9, 166.5. HRMS (ES^+) calculated for $(M + H)^+$ $C_{34}H_{45}N_6O_6$ 633.3389, found 633.3401. For the HPLC purity analysis of this compound, the method used was: 100% aqueous solution for 5 min after injection, to 60% w/v aqueous solution over 18 min as well as 100% aqueous for 5 min after injection, to 60% w/v aqueous over 43 min. The purity for the final compound was greater than 95% (HPLC, 280 nm) and was further checked by LC-MS.

CM03 was then converted to a mixed hydrochloride/formate salt in order to enhance its aqueous solubility. At a concentration of 5 mg/mL, the pH of the CM03 salt solution was 6.95.

Molecular Modeling. The crystal structure of the naphthalene diimide intramolecular telomeric G4 complexes[32,74] (PDB 2T5E, 4DA3, and 3UYH) were used as starting points to study G4−ligand interactions, in particular that with the compound MM41.[32a] The structure of the native human intramolecular DNA quadruplex with parallel-stranded propeller-type topology was extracted from the Protein Data Bank (www.rscb.org) and used for docking with CM03. The final structures were subjected to 1000 steps of conjugate gradient energy minimization to relieve any structural distortions.

The docking protocol was consistent for all systems. The chemical structures of the ligands MM41 and CM03 were sketched, built, and docked using ICM-Pro software (www.molsoft.com). Atom-centered charges were assigned using the ICFF force field.[75] Grid maps were made that encompassed the terminal quartets, central K^+ ions, and the loops. Docking was done using the automated docking module in the ICM-Pro package, employing the default parameters. The final docked conformations were chosen based on the strongest binding energy between the docked ligands and the G4. The grids were large enough to allow translation and rotation of the ligands. The top 20 plausible conformations of the ligands were then analyzed. The final docked models were chosen based on the largest interaction energy between G4 and ligand. The positively charged ions were retained within the central axis of the G4 channel and were treated as an integral part of the G4 structure.

FRET Studies. FRET DNA melting assays on MM41 and CM03 were performed using a fluorescence resonance energy transfer (FRET) assay.[76] The labeled oligonucleotides had the fluorophores 6-carboxyfluorescein (FAM) as donor and fluorophore 6-carboxytetramethyl-rhodamine (TAMRA) attached as acceptor. The sequences used are

Human telomeric G4 (F21T): 5′-FAM-d(GGG[TTAGGG]$_3$)-TAMRA-3′.

Duplex sequence 5′-FAM-d(TATAGCTATA-HEG-TATAGCTATA)-TAMRA-3′ (HEG linker, [(−CH_2-CH_2-O−)$_6$])).

HSP90a: 5′-FAM-d(GGGCCAAAGGGAAGGGGTGGG)-TAMRA-3′.

HSP90b: 5′-FAM-d(GGGCGGGCCAAAGGGAAGGGG)-TAMRA-3′.

Kras21: 5′-FAM-d(AGGGCGGTGTGGGAAGAGGGA)-TAMRA-3′.

Kras32: 5′-FAM-d(AGGGCGGTGTGGGAAGAGGGAAGAGGGGAGG)-TAMRA-3′.

Bcl-2: 5′-FAM-d(GGGCGCGGGAGGAAGGGGGCGGG)-TAMRA-3′.

The FRET probe sequences were diluted from stock to the correct concentration (400 nM) in a 60 mM potassium cacodylate buffer (pH 7.4) and then annealed by heating to 95 °C for 10 min, followed by cooling to RT in a heating block (3−3.5 h). Drug stock solutions (at 2× concentration) were prepared using 60 mM potassium cacodylate buffer (pH 7.4). Then 96-well plates (MJ Research, Waltham, MA) were prepared by aliquoting 50 μL of annealed DNA into each well, followed by 50 μL of the compound solutions. Measurements were made on a DNA Opticon Engine (MJ Research) with excitation at 450−495 nm and detection at 515−545 nm. Fluorescence readings were taken at intervals of 0.5 °C in the range 30−100 °C, with a constant temperature being maintained for 30 s prior to each reading to ensure a stable value. Final analysis of the data was carried out using a script written in the Origin 7.0 (OriginLab Corp., Northampton, MA) package and its advanced curve-fitting function for derivation of ΔT_m values.

Quantitative G4 Binding Studies. Human telomeric DNA G4 was prepared using oligonucleotides purchased from Integrated DNA

DOI: 10.1021/acs.jmedchem.7b01781
J. Med. Chem. 2018, 61, 2500−2517

Technologies (Coralville, IA, USA). The DNA purity and sequence was verified by mass spectrometry. Desalted oligonucleotide sequences were initially suspended in 150 mM NH_4OAc (pH 6.8) in nuclease-free water to yield a final concentration of 1 mM and determined spectroscopically at 260 nm using the nearest-neighbor method. The stock solution was aliquoted into 20 μL samples in 200 μL PCR tubes. Using a thermocycler, samples were heated to 98 °C for 10 min, slowly cooled for 15 min while remaining within the thermocycler, followed by an additional cooling session at RT for 30 min, and stored at 4 °C before use.

Fluorescence anisotropy measurements were obtained on a Variant Cary Eclipse fluorescence spectrophotometer (Agilent Technologies, Santa Clara, CA, USA) equipped with a polarization attachment. The excitation and emission polarizers were fixed between the light source and detector, respectively. Measurements were converted into anisotropy values by using eqs 1 and 2:

$$r = \frac{I_{vv} - \mathrm{GF} \times I_{vh}}{I_{vv} + 2 \times \mathrm{GF} \times I_{vh}} \quad (1)$$

$$\mathrm{GF} = \frac{I_{hv}}{I_{hh}} \quad (2)$$

r is the anisotropy value, I_{vv} is the fluorescence intensity of the samples when excitation and emission polarizers are aligned in vertical positions, I_{vh} is the fluorescence intensity of the samples when the excitation and emission polarizers are in vertical and horizontal positions, respectively, I_{hv} is the fluorescence intensity of compound when excitation and emission polarizers are aligned in horizontal and vertical positions, I_{vv} is the fluorescence intensity of compound when excitation and emission polarizers are aligned in vertical positions, and GF is the grating factor of the polarizers. The GF value was introduced to the equation to correct for unequal sensitivity of the excitation and emission polarizers.[77]

To determine dissociation constants, MM41 was added to a 3 mL volume of the experimental buffer (50 mM KCl, 10 mM Tris-HCl, 1 mM EDTA in nuclease-free water at 25 °C, pH 7.3) in a quartz fluorescence cuvette at a fixed concentration of 50 nM, and G4 was titrated into the cuvette. Oligonucleotide concentrations were calculated before each titration experiment and fluorophore concentrations corrected after each addition by taking dilution into account. Measurements were taken at a maximum emission wavelength of MM41 (λ_{em} = 670 nm) with excitation at λ_{ex} = 630 nm. Both excitation and emission slits were at 20 nm. Each set of measurements were taken from a 50 s average reading measurement (PMT = 630 V). The dissociation constant (K_D) of MM41 to G4 was obtained by fitting the change in anisotropy value of the compound titration using the following equation:

$$r_{observed} = r_{min} + [(r_{max} - r_{min})\{K_D + L + D - \sqrt{(K_D + L + D)^2 - 4LD}/2L\}] \quad (3)$$

r_{min} is the anisotropy value of free MM41, r_{max} is the anisotropy value of bound MM41, L is the total concentration of MM41, and D is the total concentration of G4.[77]

Direct fluorescence measurements were performed using the same instrument and experimental buffer. Both emission and excitation slits were set to 20 nm. Fluorescence was measured in a quartz fluorescence cuvette with a starting CM03 concentration of 25 nM. The amount of oligonucleotide needed for the experiment was calculated and titrated into the cuvette. Changes in maximum emission intensity of CM03 (λ_{em} = 570 nm) were observed and recorded upon binding to telomeric DNA. The curve fit equation is similar to eq 3, taking into account that fluorescence intensity values decrease upon titration (initial intensity > final intensity). The results were fitted to obtain a dissociation constant (K_D) using the fluorescence quenching equation below:

$$A = A_{initial} - [(A_{initial} - A_{final})\{K_D + L + D - \sqrt{(K_D + L + D)^2 - 4LD}/2L\}] \quad (4)$$

$A_{initial}$ is the intensity measured for free CM03, A_{final} is the intensity measured of bound CM03, K_D is the dissociation constant of the complex, L is the total concentration of CM03, and D is total concentration of G4.

Cell Culture Studies. All cell lines were purchased from ATCC and maintained in appropriate medium supplemented with 10% fetal bovine serum (Invitrogen, UK), 2 mM L-glutamine (Invitrogen, Netherlands), and other components as specified by the suppliers. Cell lines were maintained at 37 °C, 5% CO_2, and routinely passaged. Drugs were dissolved in H_2O and filtered through 0.22 μm pore-size filter units (stock 10 mM) before addition to appropriate cell line media. Cellular growth inhibition was measured using the sulforhodamine B (SRB) assay in 96-well plates as described previously.[78] The 50% inhibitory concentrations (IC_{50}) were determined by taking the mean absorbance at 540 nm for each drug concentration expressed as a percentage of the absorbance of untreated control wells.

Xenograft Studies. All animal experiments were performed in accordance with the UK Home Office Animals Scientific Procedures Act 1986 and the United Kingdom Coordinating Committee on Cancer Research Guidelines for the Welfare and Use of Animals in Cancer Research[79] and with the approval of the University College London Animal Ethics Committee. Mice had access to food and water ad libitum.

The maximum tolerated dose (MTD) studies of MM41 and CM03 were performed in CD-1 nude mice. The MTD of a single dose administered intravenously (IV) was examined, and repeat dosing was performed per week at different concentrations of MM41 (20, 25, and 30 mg/kg) and CM03 (10, 20, 30, 35, 40, 45, 50, and 60 mg/kg), with two mice per group. Compounds were administered in saline. Mice were monitored visually for signs of adverse effects over periods of up to 72 h. The maximum tolerated dose was judged to have been reached when all mice in a particular dose cohort survived in the absence of any observed ill effects for the period of the experiment.

For therapy studies, female CD-1 nude mice (2−3 months old, weighing 20−25 g) were injected subcutaneously with 5×10^6 MIA PaCa-2 cells in the right flank (unsupplemented RPMI + Matrigel). When the tumors were established (approximately 13 days, mean size 0.05 cm^3), the mice were divided into five treatment groups with eight mice/group. The MM41 and CM03 samples were dissolved directly in saline to the required concentrations and administered IV. Tumor size was measured weekly by calliper using the π-based ellipsoid volume formula (length × width × height × π/6) every 3−4 days, and the mice were also weighed and examined at the same time to determine any signs of toxicity from the drug.

Group 1:15 mg/kg of gemcitabine (Sigma), twice weekly dose.
Group 2:15 mg/kg of MM41, twice weekly dose.
Group 3:10 mg/kg of CM03, twice weekly dose.
Group 4:15 mg/kg of CM03, twice weekly dose.
Group 5: saline only, twice weekly dose.

The xenograft data was analyzed using Student's t test (GraphPad Inc.). Responses were considered to be significant for those with probabilities (p) less than 5% ($p < 0.05$). Mice were culled if there was any sign of tumor ulceration, if tumor volume exceeded 1.5 cm^3, or if a weight loss over 20% of initial body weight was observed. Samples of liver, kidney, and spleen from each animal in the CM03 (15 mg/kg) and untreated control groups were excised at the end of the therapy experiment, then fixed in 10% neutral buffered formalin for at least 48 h prior to processing and paraffin embedding. Tissue slices were stained with hematoxylin and eosin and assessed visually for any obvious differences compared with controls, indicative of toxicity and tissue damage. For the imaging study mice were anesthetized using isoflurane and imaged using the IVIS preclinical imaging system from PerkinElmer. Images were captured after 4 h following intravenous administration of CM03 using Cy5.5 excitation for 5 s.

KPC Mouse Model. KPC (*Pdx1-Cre*; *LSL-Kras*$^{G12D/+}$; *LSL-Trp53*$^{R172H/+}$) mice were described previously.[80] Mice on a mixed

DOI: 10.1021/acs.jmedchem.7b01781
J. Med. Chem. 2018, 61, 2500−2517

background were bred in-house and maintained in conventional caging with environmental enrichment, access to standard chow, and water ad libitum. Genotyping was performed by Transnetyx (Cordoba, TN, USA). Mice were monitored three times weekly and randomized to receive either 15 mg/kg of CM03, or saline control IP, twice weekly when exhibiting symptoms of PDAC (swollen abdomen, loss of body conditioning resembling cachexia, reduced mobility). Pancreatic malignancy was confirmed by abdominal palpation. Mice were culled by schedule 1 method when symptoms progressed. All animal experiments were performed under a UK Home Office license and approved by the University of Glasgow Animal Welfare and Ethical Review Board.

RNA-seq Studies. RNA-seq analyses of exposure to CM03 were undertaken at Cambridge with PANC-1 cells and at UCL with MIA PaCa-2 cells. Data merging and subsequent analyses were undertaken in Cambridge.

Cell Culture. The PDAC cell lines PANC-1 (ATCC, catalogue no. CRL-1469) and MIA PaCa-2 (ATCC, catalogue no. CRL-142) were maintained in DMEM (ThermoFisher, catalogue no. 11965092) supplemented with 10% (v/v) heat inactivated FBS (ThermoFisher) in a humidified atmosphere containing 5% CO_2 at 37 °C. Cell lines were confirmed mycoplasma free by RNA-capture ELISA, and their genotypes were certified by STR profiling.

Determination of CM03 and Gemcitabine Dosage for RNA-Seq. PANC-1 and MIA PaCa-2 cell lines were seeded overnight at 3×10^3 cells/well and 2×10^3 cells/well in 96-well plates, respectively. Next morning, cells were treated with 0−10 μM CM03 (stock 10 mM in dH_20) for 24 h. For treatment with gemcitabine-HCl (Tocris, catalogue no. 3259) (stock 50 mM in DMSO), cells were treated with 0−5 mM for 24, 48, 72, and 96 h. Cells were then incubated with 100 μL/well of CellTiter-Glo One Solution Assay reagent (Promega, catalogue no. G8461) for 30 min at RT, and luminescence was measured using a PHERAstar FS microplate reader (BMG LabTech). Cell survival curves were then plotted and GI_{50} values were calculated using GraphPad Prism version 6.00 (GraphPad Software Inc.). Error bars represent standard deviation of the mean of four technical replicates.

RNA-seq. PANC-1 (0.35×10^6 cells/well) and MIA PaCa-2 (1.5×10^6 cells/well) cell lines were seeded overnight in 60 mm plates. Next day, cells were treated with 400 nM CM03 for 6 and 24 h. For gemcitabine treatment, cells were treated for 6 and 24 h with DMSO or 30 nM, 100 nM, 300 nM, 1 μM, 3 μM, and 10 μM gemcitabine-HCL for PANC-1 cells and 30 nM, 300 nM, and 3 μM gemcitabine-HCl for MIA PaCa-2 cells. Total RNA was extracted using the Qiagen RNeasy Plus Mini Kit (ThermoFisher, catalogue no. 74134) as per the manufacturer's instructions. RNA quality (RIN > 9.0) was checked with an Aligent 2100 bioanalyzer RNA 6000 Nano Chip, and RNA concentration was quantified using a Qubit fluorometer (ThermoFisher) and Qubit RNA HS Assay Kit (Qiagen, catalogue no. Q32852). RNA-seq libraries were then generated using the Illumina Truseq RNA HT (stranded mRNA) kit (Illumina, catalogue no. RS-122−2103) as per the manufacturer's instructions and sequenced using an Illumina HiSeq4000.

RNA-Seq Analysis. Fastq raw sequencing files were preprocessed using cutadapt[81] to remove sequencing adapters and low quality sequencing tails (options −q 10) and then aligned to the human genome (GRCh37/hg19) using tophat2[82] and using the UCSC gtf file provided by Illumina iGenomes as an annotation file (http://support.illumina.com/sequencing/sequencing_software/igenome.html). Gene counts were calculated using htseq-count[83] and the same gtf file. Differential expression analysis was done using the R package edgeR.[84] Differentially expressed genes were estimated independently for both cell lines (MIA PaCa-2 and PANC-1) and for the different time points (6 and 24 h) and were then intersected to inspect the common genes. The sequencing data is available at the GEO public functional genomics data repository (https://www.ncbi.nlm.nih.gov/geo/) as GSE105083. Details of the putative G4 sequence (PQs) analysis are given in the Supporting Information.

Immunofluorescence Microscopy. BG4 and 53BP1 immunofluorescence experiments were performed essentially as described,[16,18] with slight modifications. In brief, 8×10^4 PANC-1 cells were seeded overnight on circular no. 1.5 coverslips per well in 12-well plates. Next day, cells were incubated with 400 nM CM03 (or left untreated) in 1 mL of media at 37 °C for 6 and 24 h and then fixed with 4 (v/v) % freshly prepared paraformaldehyde in 1× PBS for 10 min at RT. Coverslips were washed 1× PBS, permeabilized with 0.1% (v/v) Triton-X100 in PBS for 10 min, washed with 1× PBS, and blocked with 2% (w/v) Marvel milk (Premier Foods plc) in PBS for 1 h at 37 °C. After blocking, coverslips were incubated with BG4 (20 nM) at 37 °C for 1 h, washed three times for 5 min with PBST (0.1% (v/v) Tween 20), and then incubated with 37 °C for 1 h with rabbit α-FLAG 1:800 (CST, catalogue no. 2368) and mouse α-53BP1 1:500 (Millipore, catalogue no. MAB2803). Subsequently, all coverslips were washed as described and incubated for 30 min at 37 °C with goat α-rabbit Alexa-488 (Thermofisher, catalogue no. A-11034) and goat α-mouse Alexa-647 (ThermoFisher, catalogue no. A-21236) at 1:800 dilution. DAPI nuclear counterstain was included in the final antibody incubation. Coverslips were then rinsed three times with reverse osmosis grade water, air-dried, and mounted onto Superfrost Plus slides (ThermoFisher, catalogue no. 4951PLUS) with ProLong Diamond Antifade Mountant (Invitrogen, catalogue no. P36961). Three biological replicates were performed. *Z*-Stack images (11 steps, 0.3 μm apart) were acquired on a Nikon Eclipse TE2000E inverted microscope with a Nikon Plan Apo λ 100× NA 1.45 oil DIC H immersion objective using an Andor Neo SCC-00488 camera at 0.06 μm per pixel. Fluorescence illumination was with a xenon source and FITC, Cy5, and DAPI fluorescent filter cubes used to image BG4, 53BP1, and the nuclei, respectively. Then 10−12 *Z*-stacks were taken per replica representing approximately 50−100 nuclei. Images were deconvolved using Huygens Professional Software (Scientific Volume Imaging BV). See extended methods, immunofluorescence, for the custom protocol designed for the BG4-53BP1 foci quantification and co-localization method.

RT-qPCR Studies. MIA PaCa-2 (6 h = 2.5×10^6 and 24 h = 1.0×10^6 cells/well) and PANC-1 (6 h = 1.0×10^6 and 24 h = 0.5×10^6 cells/well) cell lines were seeded in 100 mm plates and incubated overnight. In the following day, cells were treated with 400 nM CM03, 400 nM gemcitabine, PBS, or DMSO for 6 and 24 h. Total RNA was extracted from $2-4 \times 10^6$ cells using the RNeasy mini kit (Qiagen, catalogue no. 74104), and on-column DNaseI digestion (Qiagen, catalogue no. 79254) was performed to remove residual genomic DNA. The concentration of harvested RNA was measured with a NanoDrop 2000/2000c spectrophotometer (ThermoFisher). The required amount of RNA was reverse transcribed into cDNA using a SuperScript III First-Strand Synthesis System (ThermoFisher, catalogue no. 18080051) following the manufacturer's instructions. RT-qPCR was performed using Power SYBR Green Master Mix (ThermoFisher, catalogue no. 4368706) with a 50 ng template and 150 nM primers in an AriaMx Realtime PCR System (Agilent). Primers were purchased from Eurofins Genomics or from Sigma (KiCqStart SYBR Green Primers). Data was derived from three or four independent experiments, each performed in triplicate. The C_t values were normalized to the genomic mean of three housekeeping genes *ACTB*, *GAPDH*, and *TUBB*, and the fold change was determined using $2^{-\Delta\Delta Ct}$.

Ancillary Data. The sequencing data is available at the GEO public functional genomics data repository (https://www.ncbi.nlm.nih.gov/geo/), as GSE105083. The PDB files for the "best" molecular models of MM41 and CM03 with the human DNA telomeric quadruplex are available as Supporting Information.

■ ASSOCIATED CONTENT

Supporting Information

The Supporting Information is available free of charge on the ACS Publications website at DOI: 10.1021/acs.jmedchem.7b01781.

DOI: 10.1021/acs.jmedchem.7b01781
J. Med. Chem. 2018, 61, 2500−2517

Supplementary figures and extended descriptions of the methodology and results of the RNA-seq experiments (PDF)
MIAPACA2 PANC1 degene PQs summary CM03 (XLSX)
Common degene PQs summary CM03 (XLSX)
PQs Box Whisker Plots statistics (XLS)
Degenes 300 nM gemcitabine (XLS)
KEGG pathway common degenes PQs summary CM03 (XLS)
MIAPACA2 PANC1 KEGG pathway degenes summary CM03 (XLS)
KEGG pathway degenes 300 nM gemcitabine (XLSX)
SMILES molecular formula strings (CSV)
CM03 with human telomeric G4 (PDB)
MM41 with human telomeric G4 (PDB)

AUTHOR INFORMATION

Corresponding Author

*Phone: 0044-207-753-5969. E-mail: s.neidle@ucl.ac.uk.

ORCID

Shankar Balasubramanian: 0000-0002-0281-5815
Stephen Neidle: 0000-0003-0622-6548

Present Address

○For J.A.P.: Centre of Membrane Proteins and Receptors, University of Birmingham, Birmingham B15 2TT, U.K.

Author Contributions

C.M. and K.G.Z. contributed equally to this work. In London, S.N. conceived the overall project, coordinated the various activities, analyzed the modeling data and the RNA-seq analysis performed at UCL, and oversaw writing the manuscript. C.M. and S.A.O. designed CM03, developed the synthetic route, and undertook the FRET studies, with the help of I.P. and G.Di.V. S.M.H. undertook the molecular modeling and simulation studies. M.G., R.J.B., and A.C.G.A. undertook the cell biology and RNA extraction for the RNA-seq studies at UCL. M.R., R.B.P., and S.D. undertook the xenograft studies, and J.M. and T.R.J.E. were responsible for the KPC study. A.A.A. undertook the qRT-PCR studies. T.V., S.L.T., and W.D.W. performed the quantitative binding studies in Atlanta, Georgia, USA. At Cambridge UK, K.G.Z. carried out all experiments, RNA-seq library preparation and sequencing, which was carried out by the Genomic Core service at the CRUK Cambridge Institute. G.M. designed, implemented, and performed the genomic bioinformatics analyses. D.T. and K.G.Z. designed immunofluorescence microscopy experiments, and D.T., G.M. and K.G.Z. designed the RNA-seq experiments. K.G.Z. and J.A.P. designed and quantitated the colocalization immunofluorescence microscopy experiments. All Cambridge authors interpreted the data and wrote the sequencing and immunofluorescence sections of manuscript as well as a major part of the discussion.

Notes

The authors declare no competing financial interest.

ACKNOWLEDGMENTS

Work in the S.N. laboratory has been supported by the Pancreatic Cancer Research Fund, the Medical Research Council, the Wellcome Trust, and Johnson & Johnson, with current support from the UCL Technology Fund. K.G. Z, D.T., and G.M. thank the staff of the Genomic, Light Microscopy and Biorepository core facilities at Cancer Researcher UK Cambridge Institute. S.N. thanks Tony Brooks and the staff of the UCL Genomics Facility for expert assistance with RNA-seq studies at UCL. S.B. acknowledges the support of the University of Cambridge and a Cancer Research UK programme grant. K.G.Z, D.T., and G.M. are supported by core funding from Cancer Research UK (C14303/A17197). S.B. is a Wellcome Trust Senior Investigator. We are grateful to Drs. Richard Angell and Sally Oxenford (UCL Drug Discovery Group) and Professor Daniel Hochhauser (UCL Cancer Institute) for helpful discussions. J.P.M. and T.R.J.E. acknowledge the support of the Cancer Research UK Glasgow Centre and the BSU facilities at the Cancer Research UK Beatson Institute (C596/A18076, C596/A17196).

REFERENCES

(1) Kamisawa, T.; Wood, L. D.; Itoi, T.; Takaori, K. Pancreatic cancer. *Lancet* **2016**, *388*, 73−85.

(2) Bailey, P.; Chang, D. K.; Nones, K.; Johns, A. L.; Patch, A. M.; Gingras, M. C.; Miller, D. K.; Christ, A. N.; Bruxner, T. J.; Quinn, M. C.; Nourse, C.; Murtaugh, L. C.; Harliwong, I.; Idrisoglu, S.; Manning, S.; Nourbakhsh, E.; Wani, S.; Fink, L.; Holmes, O.; Chin, V.; Anderson, M. J.; Kazakoff, S.; Leonard, C.; Newell, F.; Waddell, N.; Wood, S.; Xu, Q.; Wilson, P. J.; Cloonan, N.; Kassahn, K. S.; Taylor, D.; Quek, K.; Robertson, A.; Pantano, L.; Mincarelli, L.; Sanchez, L. N.; Evers, L.; Wu, J.; Pinese, M.; Cowley, M. J.; Jones, M. D.; Colvin, E. K.; Nagrial, A. M.; Humphrey, E. S.; Chantrill, L. A.; Mawson, A.; Humphris, J.; Chou, A.; Pajic, M.; Scarlett, C. J.; Pinho, A. V.; Giry-Laterriere, M.; Rooman, I.; Samra, J. S.; Kench, J. G.; Lovell, J. A.; Merrett, N. D.; Toon, C. W.; Epari, K.; Nguyen, N. Q.; Barbour, A.; Zeps, N.; Moran-Jones, K.; Jamieson, N. B.; Graham, J. S.; Duthie, F.; Oien, K.; Hair, J.; Grutzmann, R.; Maitra, A.; Iacobuzio-Donahue, C. A.; Wolfgang, C. L.; Morgan, R. A.; Lawlor, R. T.; Corbo, V.; Bassi, C.; Rusev, B.; Capelli, P.; Salvia, R.; Tortora, G.; Mukhopadhyay, D.; Petersen, G. M.; Munzy, D. M.; Fisher, W. E.; Karim, S. A.; Eshleman, J. R.; Hruban, R. H.; Pilarsky, C.; Morton, J. P.; Sansom, O. J.; Scarpa, A.; Musgrove, E. A.; Bailey, U. M.; Hofmann, O.; Sutherland, R. L.; Wheeler, D. A.; Gill, A. J.; Gibbs, R. A.; Pearson, J. V.; Waddell, N.; Biankin, A. V.; Grimmond, S. M. Genomic analyses identify molecular subtypes of pancreatic cancer. *Nature* **2016**, *531*, 47−52.

(3) Campbell, P. J.; Yachida, S.; Mudie, L. J.; Stephens, P. J.; Pleasance, E. D.; Stebbings, L. A.; Morsberger, L. A.; Latimer, C.; McLaren, S.; Lin, M. L.; McBride, D. J.; Varela, I.; Nik-Zainal, S. A.; Leroy, C.; Jia, M.; Menzies, A.; Butler, A. P.; Teague, J. W.; Griffin, C. A.; Burton, J.; Swerdlow, H.; Quail, M. A.; Stratton, M. R.; Iacobuzio-Donahue, C.; Futreal, P. A. The patterns and dynamics of genomic instability in metastatic pancreatic cancer. *Nature* **2010**, *467*, 1109−1113.

(4) Waddell, N.; Pajic, M.; Patch, A.-M.; Chang, D. K.; Kassahn, K. S.; Bailey, P.; Johns, A. L.; Miller, D.; Nones, K.; Quek, K.; Quinn, M. C. J.; Robertson, A. J.; Fadlullah, M. Z. H.; Bruxner, T. J. C.; Christ, A. N.; Harliwong, I.; Idrisoglu, S.; Manning, S.; Nourse, C.; Nourbakhsh, E.; Wani, S.; Wilson, P. J.; Markham, E.; Cloonan, N.; Anderson, M. J.; Fink, J. L.; Holmes, O.; Kazakoff, S. H.; Leonard, C.; Newell, F.; Poudel, B.; Song, S.; Taylor, D.; Waddell, N.; Wood, S.; Xu, Q.; Wu, J.; Pinese, M.; Cowley, M. J.; Lee, H. C.; Jones, M. D.; Nagrial, A. M.; Humphris, J.; Chantrill, L. A.; Chin, V.; Steinmann, A. M.; Mawson, A.; Humphrey, E. S.; Colvin, E. K.; Chou, A.; Scarlett, C. J.; Pinho, A. V.; Giry-Laterriere, M.; Rooman, I.; Samra, J. S.; Kench, J. G.; Pettitt, J. A.; Merrett, N. D.; Toon, C.; Epari, K.; Nguyen, N. Q.; Barbour, A.; Zeps, N.; Jamieson, N. B.; Graham, J. S.; Niclou, S. P.; Bjerkvig, R.; Grutzmann, R.; Aust, D.; Hruban, R. H.; Maitra, A.; Iacobuzio-Donahue, C. A.; Wolfgang, C. L.; Morgan, R. A.; Lawlor, R. T.; Corbo, V.; Bassi, C.; Falconi, M.; Zamboni, G.; Tortora, G.; Tempero, M. A.; Australian Pancreatic Cancer; Genome, I.; Gill, A. J.; Eshleman, J. R.; Pilarsky, C.; Scarpa, A.; Musgrove, E. A.; Pearson, J. V.; Biankin, A. V.;

DOI: 10.1021/acs.jmedchem.7b01781
J. Med. Chem. 2018, 61, 2500−2517

Grimmond, S. M.; et al. Whole genomes redefine the mutational landscape of pancreatic cancer. *Nature* **2015**, *518*, 495−501.
(5) Makohon-Moore, A. P.; Zhang, M.; Reiter, J. G.; Bozic, I.; Allen, B.; Kundu, D.; Chatterjee, K.; Wong, F.; Jiao, Y.; Kohutek, Z. A.; Hong, J.; Attiyeh, M.; Javier, B.; Wood, L. D.; Hruban, R. H.; Nowak, M. A.; Papadopoulos, N.; Kinzler, K. W.; Vogelstein, B.; Iacobuzio-Donahue, C. A. Limited heterogeneity of known driver gene mutations among the metastases of individual patients with pancreatic cancer. *Nat. Genet.* **2017**, *49*, 358−366.
(6) Jones, S.; Zhang, X.; Parsons, D. W.; Lin, J. C.-H.; Leary, R. J.; Angenendt, P.; Mankoo, P.; Carter, H.; Kamiyama, H.; Jimeno, A.; Hong, S.-M.; Fu, B.; Lin, M.-T.; Calhoun, E. S.; Kamiyama, M.; Walter, K.; Nikolskaya, T.; Nikolsky, Y.; Hartigan, J.; Smith, D. R.; Hidalgo, M.; Leach, S. D.; Klein, A. P.; Jaffee, E. M.; Goggins, M.; Maitra, A.; Iacobuzio-Donahue, C.; Eshleman, J. R.; Kern, S. E.; Hruban, R. H.; Karchin, R.; Papadopoulos, N.; Parmigiani, G.; Vogelstein, B.; Velculescu, V. E.; Kinzler, K. W. Core signaling pathways in human pancreatic cancers revealed by global genomic analyses. *Science (Washington, DC, U. S.)* **2008**, *321*, 1801−1806.
(7) Biankin, A. V.; Waddell, N.; Gingras, M. C.; Muthuswamy, L. B.; Johns, A. L.; Miller, D. K.; Wilson, P. J.; Patch, A. M.; Wu, J.; Chang, D. K.; Cowley, M. J.; Gardiner, B. B.; Song, S.; Harliwong, I.; Idrisoglu, S.; Nourse, C.; Nourbakhsh, E.; Manning, S.; Wani, S.; Gongora, M.; Pajic, M.; Scarlett, C. J.; Gill, A. J.; Pinho, A. V.; Rooman, I.; Anderson, M.; Holmes, O.; Leonard, C.; Taylor, D.; Wood, S.; Xu, Q.; Nones, K.; Fink, J. L.; Christ, A.; Bruxner, T.; Cloonan, N.; Kolle, G.; Newell, F.; Pinese, M.; Mead, R. S.; Humphris, J. L.; Kaplan, W.; Jones, M. D.; Colvin, E. K.; Nagrial, A. M.; Humphrey, E. S.; Chou, A.; Chin, V. T.; Chantrill, L. A.; Mawson, A.; Samra, J. S.; Kench, J. G.; Lovell, J. A.; Daly, R. J.; Merrett, N. D.; Toon, C.; Epari, K.; Nguyen, N. Q.; Barbour, A.; Zeps, N.; Kakkar, N.; Zhao, F.; Wu, Y. Q.; Wang, M.; Muzny, D. M.; Fisher, W. E.; Brunicardi, F. C.; Hodges, S. E.; Reid, J. G.; Drummond, J.; Chang, K.; Han, Y.; Lewis, L. R.; Dinh, H.; Buhay, C. J.; Beck, T.; Timms, L.; Sam, M.; Begley, K.; Brown, A.; Pai, D.; Panchal, A.; Buchner, N.; De Borja, R.; Denroche, R. E.; Yung, C. K.; Serra, S.; Onetto, N.; Mukhopadhyay, D.; Tsao, M. S.; Shaw, P. A.; Petersen, G. M.; Gallinger, S.; Hruban, R. H.; Maitra, A.; Iacobuzio-Donahue, C. A.; Schulick, R. D.; Wolfgang, C. L.; Morgan, R. A.; Lawlor, R. T.; Capelli, P.; Corbo, V.; Scardoni, M.; Tortora, G.; Tempero, M. A.; Mann, K. M.; Jenkins, N. A.; Perez-Mancera, P. A.; Adams, D. J.; Largaespada, D. A.; Wessels, L. F.; Rust, A. G.; Stein, L. D.; Tuveson, D. A.; Copeland, N. G.; Musgrove, E. A.; Scarpa, A.; Eshleman, J. R.; Hudson, T. J.; Sutherland, R. L.; Wheeler, D. A.; Pearson, J. V.; McPherson, J. D.; Gibbs, R. A.; Grimmond, S. M.; Kassahn, K. S.; et al. Pancreatic cancer genomes reveal aberrations in axon guidance pathway genes. *Nature* **2012**, *491*, 399−405.
(8) Siegel, R. L.; Miller, K. D.; Jemal, A. Cancer statistics, 2016. *CA-Cancer J. Clin.* **2016**, *66*, 7−30.
(9) *Statistics by Cancer Type*; Cancer Research: London, 2017; http://www.cancerresearchuk.org/health-professional/cancer-statistics/statistics-by-cancer-type/pancreatic-cancer_-_heading-Two (accessed January 6, 2017).
(10) Carmichael, J.; Fink, U.; Russell, R. C.; Spittle, M. F.; Harris, A. L.; Spiessi, G.; Blatter, J. Phase II study of gemcitabine in patients with advanced pancreatic cancer. *Br. J. Cancer* **1996**, *73*, 101−105.
(11) Von Hoff, D. D.; Ervin, T.; Arena, F. P.; Chiorean, E. G.; Infante, J.; Moore, M.; Seay, T.; Tjulandin, S. A.; Ma, W. W.; Saleh, M. N.; Harris, M.; Reni, M.; Dowden, S.; Laheru, D.; Bahary, N.; Ramanathan, R. K.; Tabernero, J.; Hidalgo, M.; Goldstein, D.; Van Cutsem, E.; Wei, X.; Iglesias, J.; Renschler, M. F. Increased survival in pancreatic cancer with nab-paclitaxel plus gemcitabine. *N. Engl. J. Med.* **2013**, *369*, 1691−1703.
(12) Conroy, T.; Desseigne, F.; Ychou, M.; Bouche, O.; Guimbaud, R.; Becouarn, Y.; Adenis, A.; Raoul, J. L.; Gourgou-Bourgade, S.; de la Fouchardiere, C.; Bennouna, J.; Bachet, J. B.; Khemissa-Akouz, F.; Pere-Verge, D.; Delbaldo, C.; Assenat, E.; Chauffert, B.; Michel, P.; Montoto-Grillot, C.; Ducreux, M. FOLFIRINOX versus gemcitabine for metastatic pancreatic cancer. *N. Engl. J. Med.* **2011**, *364*, 1817−1825.
(13) Zimmermann, G.; Papke, B.; Ismail, S.; Vartak, N.; Chandra, A.; Hoffmann, M.; Hahn, S. A.; Triola, G.; Wittinghofer, A.; Bastiaens, P. I.; Waldmann, H. Small molecule inhibition of the KRAS-PDEdelta interaction impairs oncogenic KRAS signalling. *Nature* **2013**, *497*, 638−642.
(14) Neidle, S. Quadruplex nucleic acids as novel therapeutic targets. *J. Med. Chem.* **2016**, *59*, 5987−6011.
(15) Huppert, J. L.; Balasubramanian, S. G-quadruplexes in promoters throughout the human genome. *Nucleic Acids Res.* **2007**, *35*, 406−413.
(16) Hansel-Hertsch, R.; Beraldi, D.; Lensing, S. V.; Marsico, G.; Zyner, K.; Parry, A.; Di Antonio, M.; Pike, J.; Kimura, H.; Narita, M.; Tannahill, D.; Balasubramanian, S. G-quadruplex structures mark human regulatory chromatin. *Nat. Genet.* **2016**, *48*, 1267−1272.
(17) Chambers, V. S.; Marsico, G.; Boutell, J. M.; Di Antonio, M.; Smith, G. P.; Balasubramanian, S. High-throughput sequencing of DNA G-quadruplex structures in the human genome. *Nat. Biotechnol.* **2015**, *33*, 877−881.
(18) Biffi, G.; Tannahill, D.; McCafferty, J.; Balasubramanian, S. Quantitative visualization of DNA G-quadruplex structures in human cells. *Nat. Chem.* **2013**, *5*, 182−186.
(19) Henderson, A.; Wu, Y.; Huang, Y. C.; Chavez, E. A.; Platt, J.; Johnson, F. B.; Brosh, R. M.; Sen, D.; Lansdorp, P. M. Detection of G-quadruplex DNA in mammalian cells. *Nucleic Acids Res.* **2014**, *42*, 860−869.
(20) Biffi, G.; Tannahill, D.; Miller, J.; Howat, W. J.; Balasubramanian, S. Elevated levels of G-quadruplex formation in human stomach and liver cancer tissues. *PLoS One* **2014**, *9*, e102711.
(21) (a) Monchaud, D.; Teulade-Fichou, M. P. A hitchhiker's guide to G-quadruplex ligands. *Org. Biomol. Chem.* **2008**, *6*, 627−636. 29 (b) Müller, S.; Rodriguez, R. G-quadruplex interacting small molecules and drugs: from bench towards bedside. *Expert Rev. Clin. Pharmacol.* **2014**, *7*, 663−679. (c) Islam, M. K.; Jackson, P. J.; Rahman, K. M.; Thurston, D. E. Recent advances in targeting the telomeric G-quadruplex DNA sequence with small molecules as a strategy for anticancer therapies. *Future Med. Chem.* **2016**, *8*, 1259−1290.
(22) Siddiqui-Jain, A.; Grand, C. L.; Bearss, D. J.; Hurley, L. H. Direct evidence for a G-quadruplex in a promoter region and its targeting with a small molecule to repress c-MYC transcription. *Proc. Natl. Acad. Sci. U. S. A.* **2002**, *99*, 11593−11598.
(23) Rigo, R.; Palumbo, M.; Sissi, C. G-quadruplexes in human promoters: A challenge for therapeutic applications. *Biochim. Biophys. Acta, Gen. Subj.* **2017**, *1861*, 1399−1413.
(24) (a) Boddupally, P. V.; Hahn, S.; Beman, C.; De, B.; Brooks, T. A.; Gokhale, V.; Hurley, L. H. Anticancer activity and cellular repression of c-MYC by the G-quadruplex-stabilizing 11-piperazinyl-quindoline is not dependent on direct targeting of the G-quadruplex in the c-MYC promoter. *J. Med. Chem.* **2012**, *55*, 6076−6086. (b) Brown, R. V.; Danford, F. L.; Gokhale, V.; Hurley, L. H.; Brooks, T. A. Demonstration that drug-targeted down-regulation of MYC in non-Hodgkins lymphoma is directly mediated through the promoter G-quadruplex. *J. Biol. Chem.* **2011**, *286*, 41018−41027. (c) Felsenstein, K. M.; Saunders, L. B.; Simmons, J. K.; Leon, E.; Calabrese, D. R.; Zhang, S.; Michalowski, A.; Gareiss, P.; Mock, B. A.; Schneekloth, J. S., Jr. Small molecule microarrays enable the identification of a selective, quadruplex-binding inhibitor of MYC expression. *ACS Chem. Biol.* **2016**, *11*, 139−148.
(25) Drygin, D.; Siddiqui-Jain, A.; O'Brien, S.; Schwaebe, M.; Lin, A.; Bliesath, J.; Ho, C. B.; Proffitt, C.; Trent, K.; Whitten, J. P.; Lim, J. K.; Von Hoff, D.; Anderes, K.; Rice, W. G. Anticancer activity of CX-3543: a direct inhibitor of rRNA biogenesis. *Cancer Res.* **2009**, *69*, 7653−7661.
(26) Xu, H.; Di Antonio, M.; McKinney, S.; Mathew, V.; Ho, B.; O'Neil, N. J.; Santos, N. D.; Silvester, J.; Wei, V.; Garcia, J.; Kabeer, F.; Lai, D.; Soriano, P.; Banath, J.; Chiu, D. S.; Yap, D.; Le, D. D.; Ye, F. B.; Zhang, A.; Thu, K.; Soong, J.; Lin, S. C.; Tsai, A. H.; Osako, T.; Algara, T.; Saunders, D. N.; Wong, J.; Xian, J.; Bally, M. B.; Brenton, J. D.; Brown, G. W.; Shah, S. P.; Cescon, D.; Mak, T. W.; Caldas, C.; Stirling, P. C.; Hieter, P.; Balasubramanian, S.; Aparicio, S. CX-5461 is

DOI: 10.1021/acs.jmedchem.7b01781
J. Med. Chem. 2018, 61, 2500−2517

a DNA G-quadruplex stabilizer with selective lethality in BRCA1/2 deficient tumors. *Nat. Commun.* **2017**, *8*, 14432.
(27) A Phase I/II Study of CX5461. *ClinicalTrials.gov*; U.S. National Institutes of Health: Bethesda, MD, 2016; https://clinicaltrials.gov/ct2/show/NCT02719977 (accessed Jan 7, 2017).
(28) (a) Doria, F.; Nadai, M.; Sattin, G.; Pasotti, L.; Richter, S. N.; Freccero, M. Water soluble extended naphthalene diimides as pH fluorescent sensors and G-quadruplex ligands. *Org. Biomol. Chem.* **2012**, *10*, 3830−3840. (b) Spinello, A.; Barone, G.; Grunenberg, J. Molecular recognition of naphthalene diimide ligands by telomeric quadruplex-DNA: the importance of the protonation state and mediated hydrogen bonds. *Phys. Chem. Chem. Phys.* **2016**, *18*, 2871−2877. (c) Răsădean, D. M.; Sheng, B.; Dash, J.; Pantoş, G. D. Amino-acid-derived naphthalenediimides as versatile G-quadruplex binders. *Chem. - Eur. J.* **2017**, *23*, 8491−8499. (d) Street, S.; Chin, D.; Hollingworth, G.; Berry, M.; Morales, J. C.; Galan, M. C. Divalent naphthalene diimide ligands display high selectivity for the human telomeric G-quadruplex in K^+ buffer. *Chem. - Eur. J.* **2017**, *23*, 6953−6958.
(29) (a) Nadai, M.; Cimino-Reale, G.; Sattin, G.; Doria, F.; Butovskaya, E.; Zaffaroni, N.; Freccero, M.; Palumbo, M.; Richter, S. N.; Folini, M. Assessment of gene promoter Gquadruplex binding and modulation by a naphthalene diimide derivative in tumor cells. *Int. J. Oncol.* **2015**, *46*, 369−380. (b) Lopergolo, A.; Perrone, R.; Tortoreto, M.; Doria, F.; Beretta, G. L.; Zuco, V.; Freccero, M.; Borrello, M. G.; Lanzi, C.; Richter, S. N.; Zaffaroni, N.; Folini, M. Targeting of RET oncogene by naphthalene diimide-mediated gene promoter G-quadruplex stabilization exerts anti-tumor activity in oncogene-addicted human medullary thyroid cancer. *Oncotarget* **2016**, *7*, 49649−49663.
(30) (a) Cuenca, F.; Greciano, O.; Gunaratnam, M.; Haider, S.; Munnur, D.; Nanjunda, R.; Wilson, W. D.; Neidle, S. Tri- and tetra-substituted naphthalene diimides as potent G-quadruplex ligands. *Bioorg. Med. Chem. Lett.* **2008**, *18*, 1668−1673. (b) Gunaratnam, M.; Swank, S.; Haider, S. M.; Galesa, K.; Reszka, A. P.; Beltran, M.; Cuenca, F.; Fletcher, J. A.; Neidle, S. Targeting human gastrointestinal stromal tumor cells with a quadruplex-binding small molecule. *J. Med. Chem.* **2009**, *52*, 3774−3783. (c) Hampel, S. M.; Sidibe, A.; Gunaratnam, M.; Riou, J.-F.; Neidle, S. Tetrasubstituted naphthalene diimide ligands with selectivity for telomeric G-quadruplexes and cancer cells. *Bioorg. Med. Chem. Lett.* **2010**, *20*, 6459−6463. (d) Gunaratnam, M.; de la Fuente, M.; Hampel, S. M.; Todd, A. K.; Reszka, A. P.; Schatzlein, A.; Neidle, S. Targeting pancreatic cancer with a G-quadruplex ligand. *Bioorg. Med. Chem.* **2011**, *19*, 7151−7157.
(31) Gunaratnam, M.; Cuenca, F.; Neidle, S. Naphthalene diimide compounds interacting with G-quadruplex regions in DNA. U.S. Patent 8,796,456, August 14, 2014; Eur. Patent 2227470, March 5, 2014; Jap. Patent 5366968, August 29, 2013.
(32) (a) Micco, M.; Collie, G. W.; Dale, A. G.; Ohnmacht, S. A.; Pazitna, I.; Gunaratnam, M.; Reszka, A. P.; Neidle, S. Structure-based design and evaluation of naphthalene diimide G-quadruplex ligands as telomere targeting agents in pancreatic cancer cells. *J. Med. Chem.* **2013**, *56*, 2959−2974. (b) Parkinson, G. N.; Lee, M. P. H.; Neidle, S. Crystal structure of parallel quadruplexes from human telomeric DNA. *Nature* **2002**, *417*, 876−880.
(33) Ohnmacht, S. A.; Marchetti, C.; Gunaratnam, M.; Besser, R. J.; Haider, S. M.; Di Vita, G.; Lowe, H. L.; Mellinas-Gomez, M.; Diocou, S.; Robson, M.; Šponer, J.; Islam, B.; Barbara Pedley, R.; Hartley, J. A.; Neidle, S. A G-quadruplex-binding compound showing anti-tumor activity in an in vivo model for pancreatic cancer. *Sci. Rep.* **2015**, *5*, 11385.
(34) Gopinathan, A.; Morton, J. P.; Jodrell, D. I.; Sansom, O. J. GEMMs as preclinical models for testing pancreatic cancer therapies. *Dis. Models & Mech.* **2015**, *8*, 1185−1200.
(35) Huppert, J. L.; Balasubramanian, S. Prevalence of quadruplexes in the human genome. *Nucleic Acids Res.* **2005**, *33*, 2908−2916.
(36) Todd, A. K.; Johnston, M.; Neidle, S. Highly prevalent putative quadruplex sequence motifs in human DNA. *Nucleic Acids Res.* **2005**, *33*, 2901−2907.
(37) de Sousa Cavalcante, L.; Monteiro, G. Gemcitabine: metabolism and molecular mechanisms of action, sensitivity and chemoresistance in pancreatic cancer. *Eur. J. Pharmacol.* **2014**, *741*, 8−16.
(38) Kong, D.; Zhao, Y.; Men, T.; Teng, C. B. Hippo signaling pathway in liver and pancreas: the potential drug target for tumor therapy. *J. Drug. Target.* **2015**, *23*, 125−133.
(39) Iriana, S.; Ahmed, S.; Gong, J.; Annamalai, A. A.; Tuli, R.; Hendifar, A. E. Targeting mTOR in pancreatic ductal adenocarcinoma. *Front. Oncol.* **2016**, *6*, 99.
(40) Eser, S.; Schnieke, A.; Schneider, G.; Saur, D. Oncogenic KRAS signalling in pancreatic cancer. *Br. J. Cancer* **2014**, *111*, 817−822.
(41) Trajkovic-Arsic, M.; Kalideris, E.; Siveke, J. T. The role of insulin and IGF system in pancreatic cancer. *J. Mol. Endocrinol.* **2013**, *50*, R67−74.
(42) Arlt, A.; Gehrz, A.; Mürköster, S.; Vorndamm, J.; Kruse, M. L.; Folsch, U. R.; Schafer, H. Role of NF-kappaB and Akt/PI3K in the resistance of pancreatic carcinoma cell lines against gemcitabine-induced cell death. *Oncogene* **2003**, *22*, 3243−3251.
(43) Humbert, M.; Casteran, N.; Letard, S.; Hanssens, K.; Iovanna, J.; Finetti, P.; Bertucci, F.; Bader, T.; Mansfield, C. D.; Moussy, A.; Hermine, O.; Dubreuil, P. Masitinib combined with standard gemcitabine chemotherapy: in vitro and in vivo studies in human pancreatic tumor cell lines and ectopic mouse model. *PLoS One* **2010**, *5*, e9430.
(44) Rodriguez, R.; Miller, K. M.; Forment, J. V.; Bradshaw, C. R.; Nikan, M.; Britton, S.; Oelschlaegel, T.; Xhemalce, B.; Balasubramanian, S.; Jackson, S. P. Small-molecule-induced DNA damage identifies alternative DNA structures in human genes. *Nat. Chem. Biol.* **2012**, *8*, 301−310.
(45) Rappold, I.; Iwabuchi, K.; Date, T.; Chen, J. Tumor suppressor P53 binding protein 1 (53bp1) is involved in DNA damage−signaling pathways. *J. Cell Biol.* **2001**, *153*, 613−620.
(46) Lemmens, B.; van Schendel, R.; Tijsterman, M. Mutagenic consequences of a single G-quadruplex demonstrate mitotic inheritance of DNA replication fork barriers. *Nat. Commun.* **2015**, *6*, 8909.
(47) Hessmann, E.; Johnsen, S. A.; Siveke, J. T.; Ellenrieder, V. Epigenetic treatment of pancreatic cancer: is there a therapeutic perspective on the horizon? *Gut* **2017**, *66*, 168−179.
(48) Halder, R.; Riou, J. F.; Teulade-Fichou, M. P.; Frickey, T.; Hartig, J. S. Bisquinolinium compounds induce quadruplex-specific transcriptome changes in HeLa S3 cell lines. *BMC Res. Notes* **2012**, *5*, 138.
(49) Zhang, W.; Nandakumar, N.; Shi, Y.; Manzano, M.; Smith, A.; Graham, G.; Gupta, S.; Vietsch, E. E.; Laughlin, S. Z.; Wadhwa, M.; Chetram, M.; Joshi, M.; Wang, F.; Kallakury, B.; Toretsky, J.; Wellstein, A.; Yi, C. Downstream of mutant KRAS, the transcription regulator YAP is essential for neoplastic progression to pancreatic ductal adenocarcinoma. *Sci. Signaling* **2014**, *7*, ra42.
(50) Kapoor, A.; Yao, W.; Ying, H.; Hua, S.; Liewen, A.; Wang, Q.; Zhong, Y.; Wu, C. J.; Sadanandam, A.; Hu, B.; Chang, Q.; Chu, G. C.; Al-Khalil, R.; Jiang, S.; Xia, H.; Fletcher-Sananikone, E.; Lim, C.; Horwitz, G. I.; Viale, A.; Pettazzoni, P.; Sanchez, N.; Wang, H.; Protopopov, A.; Zhang, J.; Heffernan, T.; Johnson, R. L.; Chin, L.; Wang, Y. A.; Draetta, G.; DePinho, R. A. Yap1 activation enables bypass of oncogenic Kras addiction in pancreatic cancer. *Cell* **2014**, *158*, 185−197.
(51) Shao, D. D.; Xue, W.; Krall, E. B.; Bhutkar, A.; Piccioni, F.; Wang, X.; Schinzel, A. C.; Sood, S.; Rosenbluh, J.; Kim, J. W.; Zwang, Y.; Roberts, T. M.; Root, D. E.; Jacks, T.; Hahn, W. C. KRAS and YAP1 converge to regulate EMT and tumor survival. *Cell* **2014**, *158*, 171−184.
(52) Zhou, Y.; Huang, T.; Cheng, A. S.; Yu, J.; Kang, W.; To, K. F. The TEAD family and its oncogenic role in promoting tumorigenesis. *Int. J. Mol. Sci.* **2016**, *17*, 138.
(53) Rajurkar, M.; De Jesus-Monge, W. E.; Driscoll, D. R.; Appleman, V. A.; Huang, H.; Cotton, J. L.; Klimstra, D. S.; Zhu, L. J.; Simin, K.; Xu, L.; McMahon, A. P.; Lewis, B. C.; Mao, J. The activity of Gli

DOI: 10.1021/acs.jmedchem.7b01781
J. Med. Chem. 2018, 61, 2500−2517

transcription factors is essential for Kras-induced pancreatic tumorigenesis. *Proc. Natl. Acad. Sci. U. S. A.* **2012**, *109*, E1038−1047.
(54) Jia, Y.; Xie, J. Promising molecular mechanisms responsible for gemcitabine resistance in cancer. *Genes Dis.* **2015**, *2*, 299−306.
(55) Kumar, K.; Raza, S. S.; Knab, L. M.; Chow, C. R.; Kwok, B.; Bentrem, D. J.; Popovic, R.; Ebine, K.; Licht, J. D.; Munshi, H. G. GLI2-dependent c-MYC upregulation mediates resistance of pancreatic cancer cells to the BET bromodomain inhibitor JQ1. *Sci. Rep.* **2015**, *5*, 9489.
(56) Jagadeeshan, S.; Subramanian, A.; Tentu, S.; Beesetti, S.; Singhal, M.; Raghavan, S.; Surabhi, R. P.; Mavuluri, J.; Bhoopalan, H.; Biswal, J.; Pitani, R. S.; Chidambaram, S.; Sundaram, S.; Malathi, R.; Jeyaraman, J.; Nair, A. S.; Venkatraman, G.; Rayala, S. K. P21-activated kinase 1 (Pak1) signaling influences therapeutic outcome in pancreatic cancer. *Ann. Oncol.* **2016**, *27*, 1546−1556.
(57) Han, S.; Cao, C.; Tang, T.; Lu, C.; Xu, J.; Wang, S.; Xue, L.; Zhang, X.; Li, M. ROBO3 promotes growth and metastasis of pancreatic carcinoma. *Cancer Lett.* **2015**, *366*, 61−70.
(58) Muller, M. W.; Giese, N. A.; Swiercz, J. M.; Ceyhan, G. O.; Esposito, I.; Hinz, U.; Buchler, P.; Giese, T.; Buchler, M. W.; Offermanns, S.; Friess, H. Association of axon guidance factor semaphorin 3A with poor outcome in pancreatic cancer. *Int. J. Cancer* **2007**, *121*, 2421−2433.
(59) Gara, R. K.; Kumari, S.; Ganju, A.; Yallapu, M. M.; Jaggi, M.; Chauhan, S. C. Slit/Robo pathway: a promising therapeutic target for cancer. *Drug Discovery Today* **2015**, *20*, 156−164.
(60) Cohen, R.; Neuzillet, C.; Tijeras-Raballand, A.; Faivre, S.; de Gramont, A.; Raymond, E. Targeting cancer cell metabolism in pancreatic adenocarcinoma. *Oncotarget* **2015**, *6*, 16832−16847.
(61) Li, R.; Peng, C.; Zhang, X.; Wu, Y.; Pan, S.; Xiao, Y. Roles of Arf6 in cancer cell invasion, metastasis and proliferation. *Life Sci.* **2017**, *182*, 80−84.
(62) Liang, C.; Qin, Y.; Zhang, B.; Ji, S.; Shi, S.; Xu, W.; Liu, J.; Xiang, J.; Liang, D.; Hu, Q.; Ni, Q.; Yu, X.; Xu, J. ARF6, induced by mutant Kras, promotes proliferation and Warburg effect in pancreatic cancer. *Cancer Lett.* **2017**, *388*, 303−311.
(63) Chabu, C.; Li, D. M.; Xu, T. EGFR/ARF6 regulation of Hh signalling stimulates oncogenic Ras tumor overgrowth. *Nat. Commun.* **2017**, *8*, 14688.
(64) Xie, C. G.; Wei, S. M.; Chen, J. M.; Xu, X. F.; Cai, J. T.; Chen, Q. Y.; Jia, L. T. Down-regulation of GEP100 causes increase in E-cadherin levels and inhibits pancreatic cancer cell invasion. *PLoS One* **2012**, *7*, e37854.
(65) Ying, H.; Kimmelman, A. C.; Lyssiotis, C. A.; Hua, S.; Chu, G. C.; Fletcher-Sananikone, E.; Locasale, J. W.; Son, J.; Zhang, H.; Coloff, J. L.; Yan, H.; Wang, W.; Chen, S.; Viale, A.; Zheng, H.; Paik, J. H.; Lim, C.; Guimaraes, A. R.; Martin, E. S.; Chang, J.; Hezel, A. F.; Perry, S. R.; Hu, J.; Gan, B.; Xiao, Y.; Asara, J. M.; Weissleder, R.; Wang, Y. A.; Chin, L.; Cantley, L. C.; DePinho, R. A. Oncogenic Kras maintains pancreatic tumors through regulation of anabolic glucose metabolism. *Cell* **2012**, *149*, 656−670.
(66) Selwan, E. M.; Finicle, B. T.; Kim, S. M.; Edinger, A. L. Attacking the supply wagons to starve cancer cells to death. *FEBS Lett.* **2016**, *590*, 885−907.
(67) Butler, A. M.; Scotti Buzhardt, M. L.; Li, S.; Smith, K. E.; Fields, A. P.; Murray, N. R. Protein Kinase C Zeta regulates human pancreatic cancer cell transformed growth and invasion through a STAT3-dependent mechanism. *PLoS One* **2013**, *8*, e72061.
(68) Murray, N. R.; Kalari, K. R.; Fields, A. P. Protein kinase C*ι* expression and oncogenic signaling mechanisms in cancer. *J. Cell. Physiol.* **2011**, *226*, 879−887.
(69) Thompson, M. J.; Rubbi, L.; Dawson, D. W.; Donahue, T. R.; Pellegrini, M. Pancreatic cancer patient survival correlates with DNA methylation of pancreas development genes. *PLoS One* **2015**, *10*, e0128814.
(70) Muranen, T.; Selfors, L. M.; Hwang, J.; Gallegos, L. L.; Coloff, J. L.; Thoreen, C. C.; Kang, S. A.; Sabatini, D. M.; Mills, G. B.; Brugge, J. S. ERK and p38 MAPK activities determine sensitivity to PI3K/mTOR inhibition via regulation of MYC and YAP. *Cancer Res.* **2016**, *76*, 7168−7180.
(71) Ireland, L.; Santos, A.; Ahmed, M. S.; Rainer, C.; Nielsen, S. R.; Quaranta, V.; Weyer-Czernilofsky, U.; Engle, D. D.; Perez-Mancera, P. A.; Coupland, S. E.; Taktak, A.; Bogenrieder, T.; Tuveson, D. A.; Campbell, F.; Schmid, M. C.; Mielgo, A. Chemoresistance in pancreatic cancer is driven by stroma-derived insulin-like growth factors. *Cancer Res.* **2016**, *76*, 6851−6863.
(72) Mendoza, O.; Bourdoncle, A.; Boulé, J.-B.; Brosh, J. R. M.; Mergny, J.-L. G-quadruplexes and helicases. *Nucleic Acids Res.* **2016**, *44*, 1989−2006.
(73) Day, T. A.; Layer, J. V.; Cleary, J. P.; Guha, S.; Stevenson, K. E.; Tivey, T.; Kim, S.; Schinzel, A. C.; Izzo, F.; Doench, J.; Root, D. E.; Hahn, W. C.; Price, B. D.; Weinstock, D. M. PARP3 is a promoter of chromosomal rearrangements and limits G4 DNA. *Nat. Commun.* **2017**, *8*, 15110.
(74) Collie, G. W.; Promontorio, R.; Hampel, S. M.; Micco, M.; Neidle, S.; Parkinson, G. N. Structural basis for telomeric G-quadruplex targeting by naphthalene diimide ligands. *J. Am. Chem. Soc.* **2012**, *134*, 2723−2731.
(75) Katritch, V.; Totrov, M.; Abagyan, R. ICFF: a new method to incorporate implicit flexibility into an internal coordinate force field. *J. Comput. Chem.* **2003**, *24*, 254−265.
(76) Schultes, C. M.; Guyen, B.; Cuesta, J.; Neidle, S. Synthesis, biophysical and biological evaluation of 3,6-bis-amidoacridines with extended 9-anilino substituents as potent G-quadruplex-binding telomerase inhibitors. *Bioorg. Med. Chem. Lett.* **2004**, *14*, 4347−4351.
(77) Roehrl, M. H.; Wang, J. Y.; Wagner, G. A general framework for development and data analysis of competitive high-throughput screens for small-molecule inhibitors of protein-protein interactions by fluorescence polarization. *Biochemistry* **2004**, *43*, 16056−16066.
(78) Moore, M. J.; Schultes, C. M.; Cuesta, J.; Cuenca, F.; Gunaratnam, M.; Tanious, F. A.; Wilson, W. D.; Neidle, S. Trisubstituted acridines as G-quadruplex telomere targeting agents. Effects of extensions of the 3,6- and 9-side chains on quadruplex binding, telomerase activity, and cell proliferation. *J. Med. Chem.* **2006**, *49*, 582−599.
(79) Workman, P.; Aboagye, E. O.; Balkwill, F.; Balmain, A.; Bruder, G.; Chaplin, D. J.; Double, J. A.; Everitt, J.; Farningham, D. A.; Glennie, M. J.; Kelland, L. R.; Robinson, V.; Stratford, I. J.; Tozer, G. M.; Watson, S.; Wedge, S. R.; Eccles, S. A. Guidelines for the welfare and use of animals in cancer research. *Br. J. Cancer* **2010**, *102*, 1555−1577.
(80) Hingorani, S. R.; Wang, L.; Multani, A. S.; Combs, C.; Deramaudt, T. B.; Hruban, R. H.; Rustgi, A. K.; Chang, S.; Tuveson, D. A. Trp53R172H and KrasG12D cooperate to promote chromosomal instability and widely metastatic pancreatic ductal adenocarcinoma in mice. *Cancer Cell* **2005**, *7*, 469−483.
(81) Martin, M. Cutadapt removes adapter sequences from high-throughput sequencing reads. *EMBnet J.* **2011**, *17*, 10−12.
(82) Kim, D.; Pertea, G.; Trapnell, C.; Pimentel, H.; Kelley, R.; Salzberg, S. L. TopHat2: accurate alignment of transcriptomes in the presence of insertions, deletions and gene fusions. *Genome Biol.* **2013**, *14*, R36.
(83) Anders, S.; Pyl, P. T.; Huber, W. HTSeq–a Python framework to work with high-throughput sequencing data. *Bioinformatics* **2015**, *31*, 166−169.
(84) Robinson, M. D.; McCarthy, D. J.; Smyth, G. K. edgeR: a Bioconductor package for differential expression analysis of digital gene expression data. *Bioinformatics* **2010**, *26*, 139−140.

DOI: 10.1021/acs.jmedchem.7b01781
J. Med. Chem. 2018, 61, 2500−2517